NASA TECHNICAL MEMORANDUM

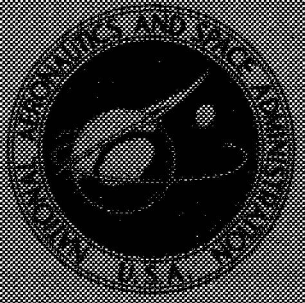

NASA TM X-2182

NASA TM X-2182

EFFECT OF EXIT AREA VARIATION ON THE PERFORMANCE OF AN AUXILIARY INLET EJECTOR NOZZLE AT MACH NUMBERS FROM 0 TO 1.27

by Bernard J. Blaha and Albert L. Johns

Lewis Research Center
Cleveland, Ohio 44135

NATIONAL AERONAUTICS AND SPACE ADMINISTRATION • WASHINGTON, D. C. • MARCH 1971

1. Report No.	2. Government Accession No.	3. Recipient's Catalog No.
NASA TM X-2182		

4. Title and Subtitle	5. Report Date
EFFECT OF EXIT AREA VARIATION ON THE PERFORMANCE OF AN AUXILIARY INLET EJECTOR NOZZLE AT MACH NUMBERS FROM 0 TO 1.27	March 1971
	6. Performing Organization Code
7. Author(s)	8. Performing Organization Report No.
Bernard J. Blaha and Albert L. Johns	E-5945
	10. Work Unit No.
9. Performing Organization Name and Address	720-03
Lewis Research Center National Aeronautics and Space Administration Cleveland, Ohio 44135	11. Contract or Grant No.
	13. Type of Report and Period Covered
12. Sponsoring Agency Name and Address	Technical Memorandum
National Aeronautics and Space Administration Washington, D.C. 20546	14. Sponsoring Agency Code

15. Supplementary Notes

16. Abstract

An auxiliary inlet ejector nozzle designed for a supersonic-cruise aircraft was tested in the Lewis 8- by 6-Foot Supersonic Wind Tunnel to determine the effect of internal expansion on the performance of the nozzle, especially at subsonic cruise. Internal area ratio was varied from 2.0 to 3.7 with a series of fixed exit areas simulating the movement of a triple-hinge, trailing-edge flap. A smaller primary area simulated subsonic cruise and dry acceleration, and a larger primary area simulated reheat acceleration. The nozzles were tested over a range of nozzle pressure ratio from 1.9 to 8.0. At a subsonic-cruise Mach number of 0.9 and a nozzle pressure ratio of 3.2, an increase in internal expansion from 2.0 to 2.9 reduced the nozzle gross thrust coefficient about 1.0 percent. A further increase in expansion ratio to 3.74, however, resulted in an additional 10-percent loss in performance.

17. Key Words (Suggested by Author(s))	18. Distribution Statement
Propulsion Nozzle Ejector	Unclassified - unlimited

19. Security Classif. (of this report)	20. Security Classif. (of this page)	21. No. of Pages	22. Price*
Unclassified	Unclassified	38	$3.00

*For sale by the National Technical Information Service, Springfield, Virginia 22151

EFFECT OF EXIT AREA VARIATION ON THE PERFORMANCE OF AN AUXILIARY INLET EJECTOR NOZZLE AT MACH NUMBERS FROM 0 TO 1.27

by Bernard J. Blaha and Albert L. Johns

Lewis Research Center

SUMMARY

An auxiliary inlet ejector nozzle designed for a supersonic-cruise aircraft was tested in the Lewis 8- by 6-Foot Supersonic Wind Tunnel to determine the effect of internal expansion on the performance, especially at subsonic cruise. Internal area ratio was varied from 2.0 to 3.74 with a series of fixed trailing-edge flaps simulating the movement of a triple-hinge, trailing-edge flap. The auxiliary inlets had 16 double-hinge, free-floating doors with the aft-door ramp angle always equal to twice the forward-door ramp angle. The nozzles were tested over a range of nozzle pressure ratio from 1.9 to 8.0. Subsonic cruise and dry acceleration were simulated with a smaller primary area, and a larger area simulated maximum reheat acceleration. Nozzle internal spacing ratio was varied from 0.458 to 0.756 and the ratio of minimum flap diameter to primary nozzle diameter was varied from 1.19 to 1.61. Corrected secondary weight flow was varied from 0 to 10 percent of the primary nozzle weight flow.

At Mach 0.9 and a nozzle pressure ratio of 3.2, an increase in internal expansion from 2.0 to 2.9 reduced the nozzle gross thrust coefficient about 1.0 percent. A further increase in expansion ratio to 3.74, however, resulted in an additional 10-percent loss in performance. For the configurations with maximum exit area, an increase in the minimum internal flap diameter combined with a corresponding decrease in spacing ratio resulted in slightly improved performance at subsonic cruise and significantly improved performance for dry and reheat acceleration.

INTRODUCTION

As part of a current program in airbreathing propulsion, the Lewis Research Center is evaluating various exhaust nozzle concepts appropriate for a supersonic-cruise aircraft. In addition to high efficiency at supersonic cruise, it is also important that these

nozzles have good subsonic-cruise and transonic acceleration performance. Requirements such as these usually necessitate extensive variations in nozzle geometry including, in the case of ejector-type nozzles, both the primary nozzle and shroud exit areas. One such nozzle being considered is the auxiliary inlet ejector. In this nozzle type, auxiliary inlets admit air from the free stream to prevent excessive overexpansion of the primary and secondary streams at low nozzle pressure ratios. Hence there is a reduced requirement for exit area variation and a corresponding reduction in projected boattail area at off-design speeds. If the tertiary flow can be handled efficiently, an overall increase in low pressure ratio performance may be realized. References 1 to 8 present the results of tests conducted on a series of isolated auxiliary inlet ejector nozzle configurations at the Lewis Research Center. These results include internal performance (from a static stand) and the effect of external flow (from the wind tunnel). Models were tested with both fixed and floating components.

To further investigate the reduced requirement for exit area variation caused by tertiary air with an isolated auxiliary inlet ejector nozzle, especially at subsonic-cruise conditions, a series of fixed trailing-edge flaps were tested utilizing the nozzle described in reference 4. These tests were conducted in the 8- by 6-Foot Supersonic Wind Tunnel over a Mach number range from 0 to 1.27 at 0° angle of attack. This nozzle incorporated 16 floating double-hinge doors. The fixed trailing-edge flaps used here simulated the movement of a triple-hinge flap and represented internal area ratio variations from 2.0 to 3.74 with corresponding boattail angles of 7° and 0°. Internal spacing ratio varied from 0.458 to 0.756 and the ratio of minimum flap diameter to primary nozzle diameter varied from 1.19 to 1.61. Nozzle pressure ratio was varied from 1.9 to 8.0 and secondary-weight-flow ratio was varied from 0 to 10 percent of the primary nozzle weight flow. Primary nozzle configurations simulated engine power settings representing subsonic cruise, dry acceleration, and maximum reheat acceleration. Dry air at room temperature was used for both primary and secondary weight flow.

APPARATUS AND PROCEDURE

Jet Exit Model

A schematic of the model installed in the 8- by 6-Foot Supersonic Wind Tunnel is shown in figure 1. Details of the internal geometry, airflow passages, and thrust-measuring system are shown. The grounded portion of the model was an 8.5-inch (21.59-cm) diameter cylinder with an ogive nose, and was supported from the tunnel ceiling by a vertical strut. The metric portion, which included the primary and secondary air bottles, was attached through cantilevered flow tubes from external supply

manifolds. The primary air bottle was supported by front and rear bearings. The secondary air passed through an annular ring around the primary nozzle. The nozzle axial forces, which included secondary and tertiary flow effects as well as external flow effects, were transmitted to a load cell located in the nose of the model. General boundary layer and external flow characteristics of this jet exit model are described in references 9 and 10. The primary and secondary flows utilized air at room temperature and were measured by means of standard ASME flowmetering orifices located in the external supply lines. As mentioned previously, thrust-minus-drag measurements were obtained from the load-cell readout of the axial forces acting on the metric portion of the model. These forces were then corrected for internal tare forces, determined from the measured tare pressures shown in figure 1. Static calibrations of the load cell were obtained by applying known forces to the nozzle. A water-cooled jacket surrounded the load cell and maintained a constant temperature of 90° F ($\sim 550^{\circ}$ R) to eliminate errors due to variations in temperature from aerodynamic heating. The external surface of the metric portion of the model begins at station 93.65 inches (238 cm). The frictional force acting on the portion of the nozzle between stations 93.65 and 122.84 inches (238 and 312 cm) was not charged to the nozzle. Its magnitude was estimated, by using conventional techniques, as a function of free-stream Mach number and Reynolds number, and this correction was applied to the load-cell force.

Two choke plates were utilized to reduce the pressure and to improve the profile of the internal flow approaching the primary nozzle inlet. The ideal jet thrust of the primary was calculated from the measured mass-flow rate expanded isentropically from the measured total pressure P_7 to free-stream ambient pressure p_0. This value was then used to determine the nozzle measured gross thrust coefficient, defined as $(F - D)/F_{i,p}$.

Nozzle Design and Instrumentation

A schematic diagram of the auxiliary inlet ejector is shown in figure 2, along with a listing of the basic nozzle parameters. The symbols are defined in appendix A. The ejector was assembled from three basic components: a primary nozzle (which simulated a J85-GE-13 nozzle), a floating auxiliary inlet door section, and a fixed trailing-edge-flap section. The primary nozzle was tested with two flow diameters to simulate either subsonic cruise and dry acceleration or reheat acceleration. Three fixed-geometry, trailing-edge-flap sections were investigated, hereinafter known as intermediate, supersonic, and thin flaps. These flaps are parametric variations from the base line configuration of reference 2 and represent fixed exit areas simulating the movement of a variable triple-hinge nozzle with an exit area in a semi-open (intermediate) and a full-open (supersonic and thin) position. The larger exit areas represented by these flaps were desired to investigate the overexpansion losses incurred, especially at the lower nozzle

pressure ratios. The intermediate flap had a 7° boattail angle, while the supersonic and thin flaps had 0° boattail angles. The projected area of the 7° boattail was 22 percent of the maximum nacelle projected area. The thin flap was similar to the supersonic flap except for an increased minimum internal diameter and a corresponding decrease in spacing ratio s/d_8. The thin flap represents an alternate means of varying the nozzle geometry besides varying d_9. With the increased minimum diameter and decreased spacing ratio, the secondary and tertiary flow passages are altered, which may improve the internal flow characteristic of the nozzle. These trailing-edge-flap configurations, along with the two primary nozzle diameters, represented internal area ratio variations from 2.07 to 3.74 and internal spacing ratio variations from 0.458 to 0.756. The minimum flap diameter to primary nozzle diameter ratio varied from 1.19 to 1.61.

Shown in figure 3 are the theoretical overexpansion areas for the three flaps investigated, as a function of nozzle pressure ratio. The overexpansion area is defined as the difference between the nozzle exit area A_9 and the fully expanded primary jet area. Also shown are the auxiliary inlet door flow areas for the doors in the full-open position. With the small primary nozzle (fig. 3(a)), the overexpansion area exceeds the open-door area at almost all conditions. With the larger primary nozzle (fig. 3(b)), the overexpansion area exceeds the open-door area for pressure ratios less than 3.9 with the intermediate flap and for pressure ratios less than 5.6 for the supersonic and thin flaps.

The dimensions and instrumentation locations of the trailing-edge flaps are shown in figure 4. A row of static-pressure orifices were installed on the internal surface of the flaps at the angular coordinate position $\varphi = 90^{\circ}$, as viewed in the upstream direction. On the intermediate flap a row of orifices was installed on the boattail at an angular coordinate position $\varphi = 180^{\circ}$. In both cases the orifices were located at the centroids of equal annular areas such that the resultant axial forces could be readily calculated. The nozzle installed in the wind tunnel is shown in figures 4(a-3) and (b-3) with the intermediate and supersonic flaps, respectively.

The primary nozzle, which was modeled from a J85-GE-13 variable-area primary nozzle, is shown in figure 5. Secondary air was directed through 12 slots in a ring which simulatel the primary nozzle actuator blockage. As mentioned previously, two different throat areas were used. The smaller throat area corresponded to an area required during subsonic cruise and dry acceleration, while the larger area corresponded to an area required during reheat acceleration. The measured flow coefficients C_d were 0.977 and 0.985 for the small and large primaries, respectively. The primary nozzle static-pressure instrumentation is also shown in figure 5. A row of pressure orifices was installed on the primary flap at the angular coordinate position of $\varphi = 90^{\circ}$ as viewed in the upstream direction. One orifice was installed on the nozzle lip. These orifices were also located at the centroids of equal annular areas. The primary nozzle is shown in figure 5(c).

Details of the auxiliary inlets are shown in figure 6. Figure 6(a) shows the dimensions of the floating double-hinge door geometry, and figure 6(b) shows the instrumentation. Sixteen equally spaced doors were mounted in a continuous circular ring which was divided into doors by 16 equally spaced struts. The space between each strut was 1.3 inches (3.3 cm). The doors were aerodynamically actuated; however, they were synchronized to reduce any circumferential nonuniformities. They were also constrained to move with a 2/1 door angle ratio between the aft-door and forward-door ramp angles. The door cross-sectional flow area was considered to be the sum of 16 areas, each 1.3 inches (3.3 cm) in width, with a height measured normal to the door at the trailing edge of the door. As seen previously in figure 3 the total tertiary flow area to exit area ratio A_{ter}/A_9 varied from 0 (closed doors) to 0.458 (open doors and intermediate flaps). The door instrumentation consisted of a row of static-pressure orifices located at the angular coordinate position of 180°. These orifices were installed such that the movement of the doors was not impeded.

The instrumentation at the primary nozzle inlet station is shown in figure 7. Typical total-pressure profiles measured at this station are shown in figure 8. The nozzle inlet total pressure P_7 was obtained by integrating the pressures measured with the rake, which was area-weighted. The flow was assumed to be circumferentially uniform. The secondary total pressure was measured somewhat further downstream at a station within the simulated primary nozzle actuator mechanism, as indicated in figures 1 and 5.

Procedure

The nozzle configurations were tested in the 8- by 6-Foot Supersonic Wind Tunnel over a Mach number range from 0 to 1.27 at 0° angle of attack. In figure 9 nozzle pressure ratio P_7/p_0 is presented as a function of flight Mach number for a typical supersonic-cruise turbojet nozzle installation. This schedule was used as a guide for setting pressure ratio at each Mach number for the various simulated power settings. At each Mach number, data were taken at several pressure ratios around the values shown in figure 9 at a nominal value of corrected secondary-weight-flow ratio. Also, at various selected pressure ratios shown in figure 9, for a Mach number and power setting, data were also obtained over a range of corrected secondary-weight-flow ratio from 0 to approximately 0.10.

The basic data for all the model configurations, consisting of gross thrust coefficients and pumping characteristics, are presented in appendix B. These data were used in conjunction with the pressure ratio - Mach number schedule of figure 9 to present the nozzle performance in the section RESULTS AND DISCUSSION.

RESULTS AND DISCUSSION

The effects of fixed trailing-edge-flap geometry on nozzle gross thrust coefficient and secondary total-pressure recovery requirements are presented in figure 10 as a function of free-stream Mach number. Data are presented for the simulated subsonic-cruise, dry-acceleration, and reheat-acceleration engine power settings at the nozzle pressure ratios shown in figure 9. Corrected secondary-weight-flow ratio was 0.04 except for the reheat-acceleration condition where data for both ratios of 0.04 and 0.08 are presented. The flagged data were obtained from the faired data presented in appendix B. In figure 10 the symbols are shaded to give an indication of the position of the floating auxiliary inlet doors at each condition. This information was obtained from visual observation of the model through a television system during the testing. The open symbols indicate that the doors were full open and the half-solid symbols indicate that the doors were in travel somewhere between the open and closed positions. Solid symbols indicate that the doors were closed. No data are presented near Mach 1.1 due to model blockage interference effects that exist on the model, as discussed in reference 10.

The results shown in figure 10 indicate that nozzle performance is a function of internal area ratio, door position, spacing ratio, boattail angle, and diameter ratio (trailing-edge-flap geometry), as well as of free-stream Mach number and simulated engine power condition. At subsonic cruise (fig. 10(a)), the auxiliary inlet doors were open at all conditions. The supersonic and thin flaps had similar gross thrust coefficients that were from 6 to 12 percent below the performance of the intermediate flap, even though the intermediate flap had a 7° boattail. This probably resulted from the more severe overexpansion losses experienced with the larger area ratio configurations. The flow through the open auxiliary inlet doors with the supersonic and thin flaps was evidently not sufficient to compensate for the large area ratio. The performance of the intermediate flap at subsonic-cruise conditions, although better than the others, was still somewhat low, with a gross thrust coefficient of about 0.88. This flap was also somewhat overexpanded at the lower nozzle pressure ratios, and, as seen previously in figure 3, the door area was less than the theoretical overexpansion area at these conditions and therefore apparently could not provide sufficient tertiary flow. The secondary total-pressure recovery required at subsonic-cruise nozzle pressure ratios was less with the thin flap than with the others because of the larger internal diameter ratio.

At dry-acceleration conditions (fig. 10(b)), the thrust performance of the intermediate and thin flaps was comparable and considerably above that of the supersonic flap, especially at the high subsonic speeds. As seen from the data, the floating auxiliary inlet doors ranged from open to closed. The doors with the thin flap were full open up to Mach 0.95, while those with the supersonic flap were only partially open up to Mach 0.7. The full-open doors with the thin flap therefore allowed more tertiary flow to enter,

which evidently helps to prevent overexpansion of the primary flow. The thin flap also provides less projected area in the overexpanded region of the primary and more projected area in the primary base region, where pressures are near ambient. At takeoff conditions the performance of all three flaps is similar and quite high, with a gross thrust coefficient of about 0.99. At this condition, the auxiliary inlet doors are full open with all three flaps, evidently providing enough tertiary flow to adequately prevent the overexpansion of the primary flow. At dry acceleration the thin flap again had the best pumping characteristics.

Similar results are apparent at reheat-acceleration conditions with the larger primary nozzle (figs. 10(c) and (d)). The thin-flap thrust performance again is better than for the supersonic flap even though they have the same internal expansion ratio. As seen in figure 10(d) for the thin flap at Mach numbers 0.6, 0.7, and 0.8, the auxiliary inlet doors were fully open. This apparently resulted from the larger minimum internal diameter of the thin flap, which provided better pumping and near ambient pressures in the primary base region. This was not completely reflected in the secondary flow characteristics presented in figure 10(d) because the flow was restricted in the simulated primary nozzle at these high flow rates. With the doors open the tertiary flow helped somewhat to prevent the overexpansion of the primary flow and resulted in higher nozzle performance. At the higher speeds the auxiliary inlet doors with the thin flaps were closed, but as mentioned previously this flap provides less projected area in the overexpanded region of the primary than does the supersonic flap and consequently had better performance. Again, at reheat conditions, the thin flap had better pumping characteristics than the other flap configurations.

The effect of internal expansion ratio on nozzle gross thrust coefficient is presented in figure 11. Data are presented from the three fixed flap configurations tested here and another fixed flap configuration tested previously on a similar auxiliary inlet nozzle in the 8- by 6-Foot Supersonic Wind Tunnel (ref. 2). This configuration had a 15° boattail, which represented a fully closed triple-hinge flap that was fixed in a closed position for subsonic operation. The projected boattail area was 47 percent of the simulated nacelle area. This flap resulted in an internal expansion ratio A_9/A_8 of 2.0 with the small primary and 1.42 with the large primary. In figure 11 comparisons are made at Mach 0.9 for the various simulated engine power conditions, and again the symbols are shaded to indicate door position. As seen in figure 11 an increase in internal expansion from 2.0 to 2.9 at subsonic cruise (fig. 11(a)) resulted in the floating doors changing from partial to full open and reduced the nozzle gross thrust coefficient only 1.0 percent. A further increase in expansion ratio to 3.74, however, resulted in an additional 10-percent loss in performance. Similar results can be seen at the other simulated engine power conditions (figs. 11(b) and (c)). With a nozzle area ratio of 3.74 at nonreheat conditions and 2.65 at reheat conditions, an increase in the minimum internal diameter of

the trailing-edge flap and a corresponding decrease in nozzle internal spacing ratio resulted in slightly increased performance at subsonic-cruise conditions (about 1 percent) and significantly increased performance at dry and maximum reheat acceleration (7.2 and 5 percent, respectively). These results were also seen previously in figure 10. These increases in thrust performance probably resulted from the increased minimum internal flap diameter and full-open doors allowing more tertiary flow with the thin flap at subsonic cruise (fig. 11(a)) and, as seen previously, from the floating doors remaining open to a higher Mach number with the thin flap at dry acceleration (fig. 11(b)). At reheat acceleration (fig. 11(c)) the thinner flap provides less projected area in the overexpanded region of the primary and more projected area in the primary base region, where pressures are near ambient.

Internal and external static-pressure distributions on the trailing-edge flaps are presented in figure 12 at a free-stream Mach number of 0.9. Data are again presented for the simulated subsonic-cruise, dry-acceleration, and reheat-acceleration power settings. At subsonic cruise (fig. 12(a)) the internal pressures are low near the minimum diameter and then recompress toward free-stream static aft in the nozzle. This type of distribution indicates that the secondary and tertiary flow have helped to separate the primary flow from the shroud wall and consequently reduce the overexpansion effects. At dry- and reheat-acceleration conditions (figs. 12(b) to (d)), the internal pressure distributions indicate a severe overexpansion of the flow, with pressures well below free-stream static on the downstream-facing surface. The pressures on the intermediate flap, however, are generally higher for most conditions, and consequently this flap results in less overexpansion loss. At dry acceleration (fig. 12(b)) the pressures on the internal downstream-facing surface of the thin flap were more comparable to those on the intermediate flap. As seen before in figures 10 and 11, at this condition the auxiliary inlet doors remained open with the thin flap and were closed with the others. Therefore the tertiary air helped to reduce the overexpansion with this flap, resulting in the higher internal pressures. As stated previously, the thin flap evidently has two advantages at these conditions: (1) it permits more tertiary flow, thereby more efficiently reducing overexpansion; and (2) it trades projected area in the overexpansion region for area in the primary base region, where pressures are nearly ambient. Therefore a more cylindrical ejector appears to be more efficient at overexpanded conditions.

At the reheat-acceleration conditions (figs. 12(c) and (d)), the pressures on the internal upstream-facing surface were higher than free-stream static, especially with the intermediate and supersonic flaps. As can be seen from figure 10 and from subsequent figures 13 and 14, these high pressures are of the same order of magnitude as the secondary total pressure and the pressures on the primary nozzle flap and in the base region under the auxiliary inlet doors. It must be noted again that the doors were closed at these conditions. Therefore, these higher pressures acting on opposite facing surfaces of nearly equal areas contribute little to the overall nozzle performance.

Pressure distributions on the external surface of the floating auxiliary inlet doors and on the primary nozzle flap at subsonic-cruise conditions and a free-stream Mach number of 0.9 are presented in figure 13. Data are presented for the three trailing-edge-flap geometries and free-stream static is shown for reference. As seen in figure 10, at these conditions the floating doors were full open. The pressures are slightly below free-stream static on the upstream door, which has little projected area, and are almost free-stream static on the downstream door. The pressures on the doors with the thin trailing-edge-flap are generally slightly lower than with the others. Similar results are seen on the primary nozzle flap. Pressures on the primary nozzle flap and under the closed doors at reheat acceleration and a free-stream Mach number of 0.9 are presented in figure 14. With the intermediate and supersonic flap the pressures are about constant and well above free-stream static. The pressures with the thin flap were near free-stream static. These results correlate with the pressures seen on the upstream-facing surface of the trailing-edge flaps in figure 12 and, as mentioned previously, correlate with the secondary total pressure.

The trailing-edge-flap pressure forces are presented in figure 15 for the various simulated engine power conditions at a free-stream Mach number of 0.9. These forces are ratioed to the ideal thrust of the primary and are presented to indicate whether the force would be a thrust or a drag. It must be noted, however, that these are only the forces on the trailing-edge flap and do not represent all the forces contributing to the performance of the nozzle. These forces do indicate, however, where some of the thrust losses occur for these flaps. At subsonic cruise and dry acceleration it is evident from figure 15 that a large portion of the performance losses occurred on the internal downstream-facing surface of the flap. This is evidently the result of nozzle overexpansion. At reheat acceleration the forces on the internal upstream-facing surface of the trailing-edge-flap seem to be significant for the intermediate and supersonic flaps. It must be noted, however, that at this condition the floating auxiliary inlet doors were closed (fig. 10); and as seen previously in figure 14, the pressures on the primary nozzle flap and under the doors were high. Therefore the forces in this region tend to oppose one another; and since they are similar in magnitude, they tend to cancel. Again the predominant performance losses generally occur on the internal downstream-facing surface of the trailing-edge flap. At these conditions these losses are generally smaller than those incurred at subsonic cruise and dry acceleration. This resulted from the smaller degree of overexpansion at reheat conditions due to the smaller internal expansion ratio and higher nozzle pressure ratios. These results therefore correlate with the results seen in figures 10 to 14.

SUMMARY OF RESULTS

An auxiliary inlet ejector nozzle designed for a supersonic-cruise aircraft was tested in the Lewis 8- by 6-Foot Supersonic Wind Tunnel to determine the effect of internal expansion on the performance, especially at subsonic cruise. Internal area ratio was varied from 2.0 to 3.74 with a series of four fixed trailing-edge flaps simulating the movement of a triple-hinge, trailing-edge flap. One flap (supersonic) simulated a supersonic-cruise configuration with a 0° boattail angle and an internal expansion ratio of 3.74 at nonreheat conditions and 2.65 at reheat conditions. Another flap (intermediate) simulated an intermediate configuration with a 7° boattail angle and had internal expansion ratios of 2.91 and 2.07 at nonreheat and reheat conditions, respectively. A third flap (thin) was similar to the supersonic flap but had an increased minimum internal diameter ratio. Data from a subsonic-cruise configuration tested previously in the wind tunnel were also used for comparison. This flap had a 15° boattail and internal expansion ratios of 2.0 and 1.42 at nonreheat and reheat conditions, respectively. Tests were conducted over a range of Mach numbers from 0 to 1.27 at 0° angle of attack. Nozzle internal spacing ratio was varied from 0.458 to 0.756 and the ratio of minimum flap diameter to primary nozzle diameter was varied from 1.19 to 1.61. Nozzle pressure ratio was varied from 1.9 to 8.0, and secondary weight flow was varied from 0 to 10 percent of the primary nozzle weight flow. Subsonic-cruise, dry-acceleration, and maximum-reheat-acceleration power settings were simulated. The following observations were made:

1. An increase in internal expansion from 2.0 to 2.9 at subsonic cruise (Mach 0.9 and a nozzle pressure ratio of 3.2) with a corresponding reduction in boattail angle from 15° to 7° resulted in the floating doors changing from partial to full open and reduced the nozzle gross thrust coefficient by only 1.0 percent. A further increase in expansion ratio to 3.74 (0° boattail angle) with the floating doors full open resulted in an additional 10-percent loss in performance.

2. Performance losses observed with the larger area ratios and lower pressure ratios resulted primarily from the low pressures generated internally on the downstream-facing surface of the trailing-edge flap (overexpansion losses).

3. For the flap configurations with maximum exit area, an increase in the minimum internal diameter (with a corresponding decrease in spacing ratio) resulted in slightly increased performance at subsonic-cruise conditions and significantly increased performance at dry and maximum reheat acceleration. The better pumping of the thin flap kept the floating doors open at subsonic cruise and dry acceleration, thereby reducing overexpansion (from that observed with a smaller minimum diameter). The thinner flap had

a smaller projected area in the region of primary flow overexpansion and more projected area in the primary base region, where pressures are near ambient.

Lewis Research Center,
National Aeronautics and Space Administration,
Cleveland, Ohio, October 27, 1970,
720-03.

APPENDIX A

SYMBOLS

A	projected area
C_d	primary nozzle flow coefficient
C_p	static-pressure coefficient, $(p_x - p_0)/q_0$
D	drag
d	model diameter
F	thrust
L	length from primary nozzle exit to nozzle exit
l	length of primary nozzle flap
M	Mach number
P	total pressure
p	static pressure
q	dynamic pressure
R	radius of primary flow duct at nozzle station 7
r	radial dimension
s	axial distance from primary nozzle exit to minimum secondary shroud diameter
T	total temperature
w	weight-flow rate
x	axial distance coordinate
β	boattail angle
$\omega\sqrt{\tau}$	corrected secondary-weight-flow-rate ratio, $(w_s/w_p)\sqrt{T_s/T_p}$
φ	angular position coordinate

Subscripts:

e	outside edge
i	ideal
max	maximum
OE	overexpansion
p	primary
s	secondary
ter	tertiary
u	upstream
x	condition at distance x

Stations:

0	free stream
7	nozzle inlet
8	nozzle throat
9	nozzle exit

APPENDIX B

BASIC PERFORMANCE DATA

The basic performance data for the three trailing-edge-flap configurations are presented as a function of nozzle pressure ratio in figures 16 to 18. Nozzle gross thrust coefficient and secondary-to-primary total-pressure ratios are presented for a nominal value of corrected secondary-weight-flow ratio. The basic performance data for the three trailing-edge flaps are presented as a function of corrected secondary-weight-flow ratio in figures 19 to 21. Nozzle gross thrust coefficient and secondary-to-primary total-pressure ratio are presented for values of Mach number and pressure ratio as obtained from figure 9.

REFERENCES

1. Shrewsbury, George D.; and Jones, John R.: Static Performance of an Auxiliary Inlet Ejector Nozzle for Supersonic-Cruise Aircraft. NASA TM X-1653, 1968.

2. Johns, Albert L.; and Steffen, Fred W.: Performance of an Auxiliary Inlet Ejector Nozzle With Fixed Inlet Doors and Triple-Hinge Trailing-Edge Flap. NASA TM X-2034, 1970.

3. Johns, Albert L.; and Steffen, Fred W.: Performance of an Auxiliary Inlet Ejector Nozzle With Fixed Doors and Single-Hinge Trailing-Edge Flap. NASA TM X-2027, 1970.

4. Johns, Albert L.: Performance of an Auxiliary Inlet Ejector Nozzle With Floating Inlet Doors and Floating Single-Hinge Trailing-Edge Flaps. NASA TM X-2173, 1971.

5. Steffen, Fred W.; and Johns, Albert L.: Performance of a Fixed Geometry Wind Tunnel Model of an Auxiliary Inlet Ejector With a Clamshell Flow Diverter From Mach 0 to 1.2. NASA TM X-2037, 1970.

6. Bresnahan, Donald L.: Performance of an Aerodynamically Positioned Auxiliary Inlet Ejector Nozzle at Mach Numbers From 0 to 2.0. NASA TM X-2023, 1970.

7. Mansour, Ali H.; and Burley, Richard R.: Internal Thrust and Pumping Performance of an Auxiliary Inlet Ejector Nozzle With Clamshell Thrust Reverser. NASA TM X-52621, 1969.

8. Burley, Richard R.; and Mansour, Ali H.: Static Performance of an Auxiliary Inlet Ejector Nozzle Using an Afterburning Turbojet Gas Generator. NASA TM X-1999, 1970.

9. Harrington, Douglas E.: Jet Effects on Boattail Pressure Drag of Isolated Ejector Nozzles at Mach Numbers From 0.60 to 1.47. NASA TM X-1785, 1969.

10. Blaha, Bernard J.; and Bresnahan, Donald L.: Wind Tunnel Installation Effects on Isolated Afterbodies at Mach Numbers From 0.56 to 1.5. NASA TM X-52581, 1969.

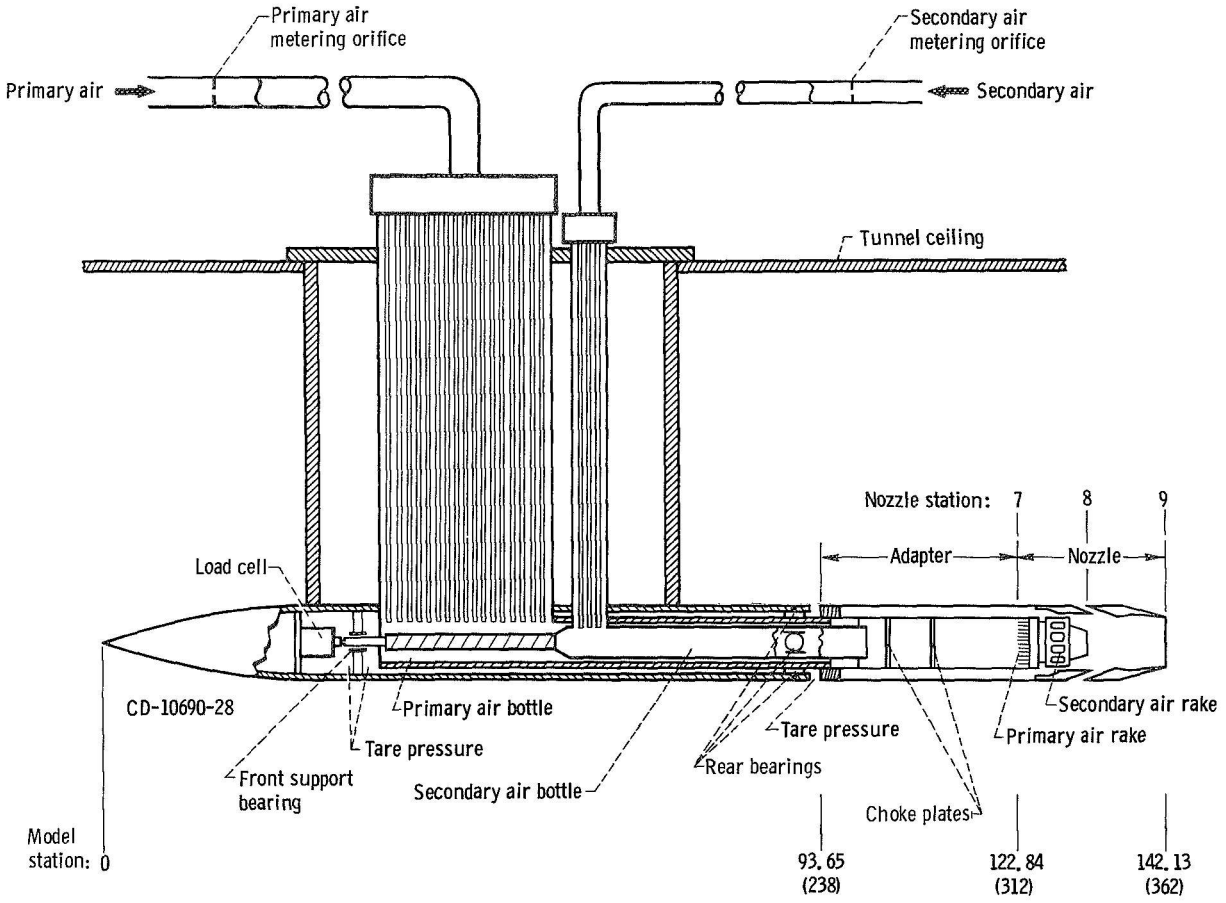

Figure 1. - Schematic of nozzle support model and air supply systems. Dimensions are in inches (cm).

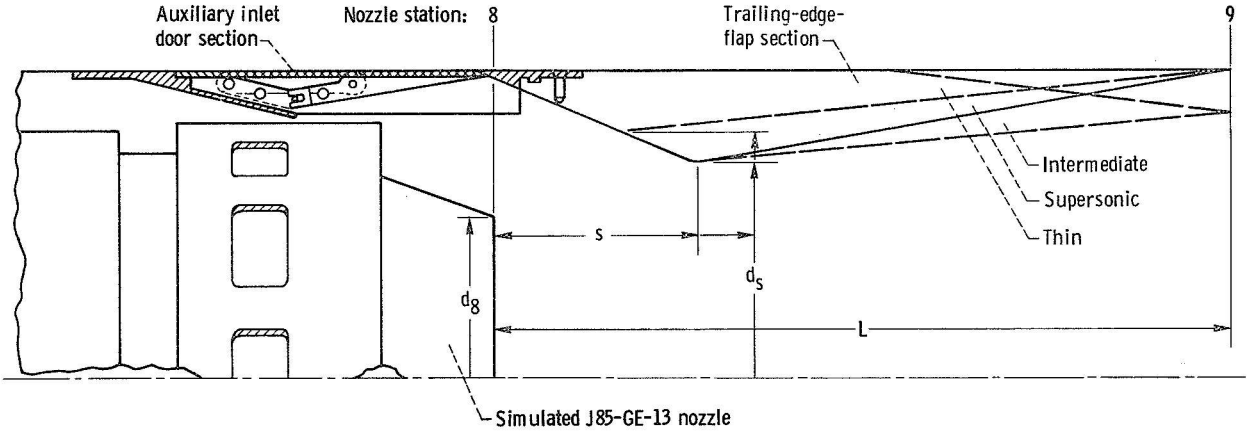

Trailing-edge flap	Primary nozzle configuration	A_8/A_{max}*	Flight simulation	Internal area ratio, A_9/A_8	Spacing ratio, s/d_8	Diameter ratio, d_s/d_8	Flap length ratio, L/d_8
Intermediate	small	0.267	No reheat	2.91	0.756	1.41	2.35
	large	.373	Reheat	2.07	.702	1.19	2.06
Supersonic	small	0.267	No reheat	3.74	0.756	1.41	2.35
	large	.373	Reheat	2.65	.720	1.19	2.06
Thin	small	0.267	No reheat	3.74	0.494	1.61	2.35
	large	.373	Reheat	2.65	.458	1.36	2.06

* Ratio of nozzle throat to maximum nacelle area

Figure 2. - Basic nozzle parameters.

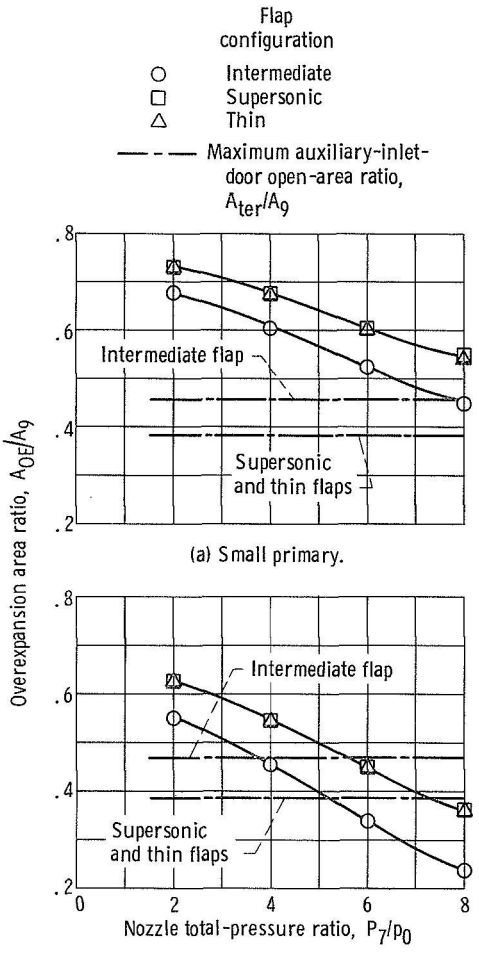

(a) Small primary.

(b) Large primary.

Figure 3. - Theoretical flap overexpansion ratio.

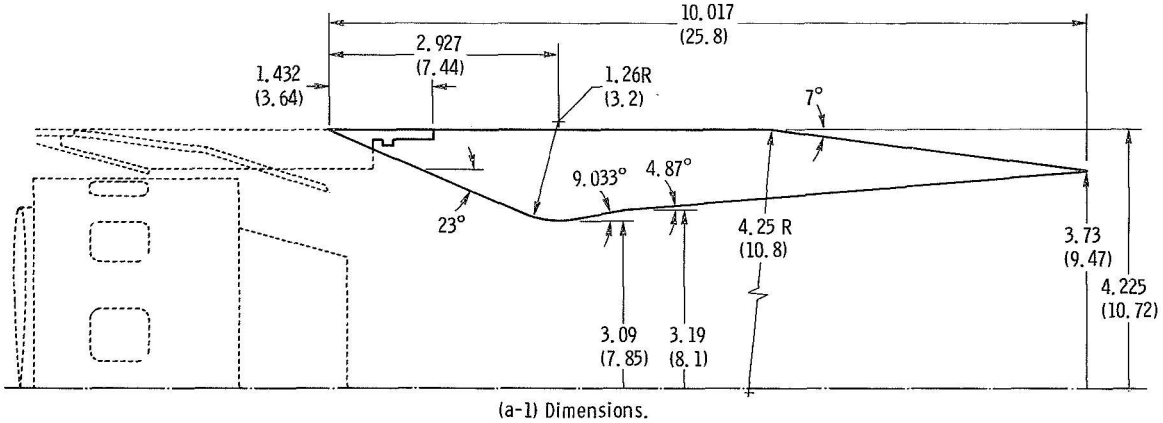

(a-1) Dimensions.

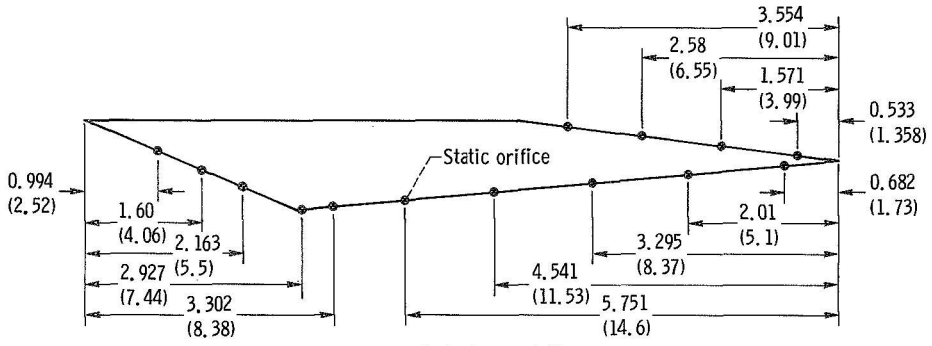

(a-2) Instrumentation.

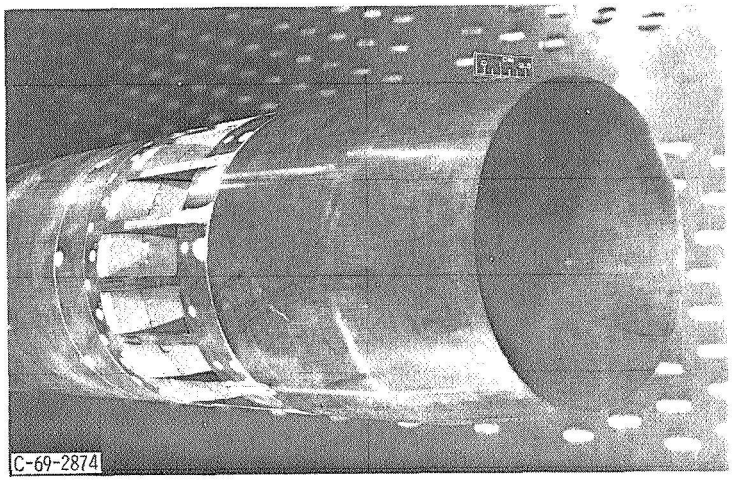

(a-3) Installed in wind tunnel.

(a) Intermediate flap.

Figure 4. - Details of fixed trailing-edge flaps. Dimensions are in inches (cm).

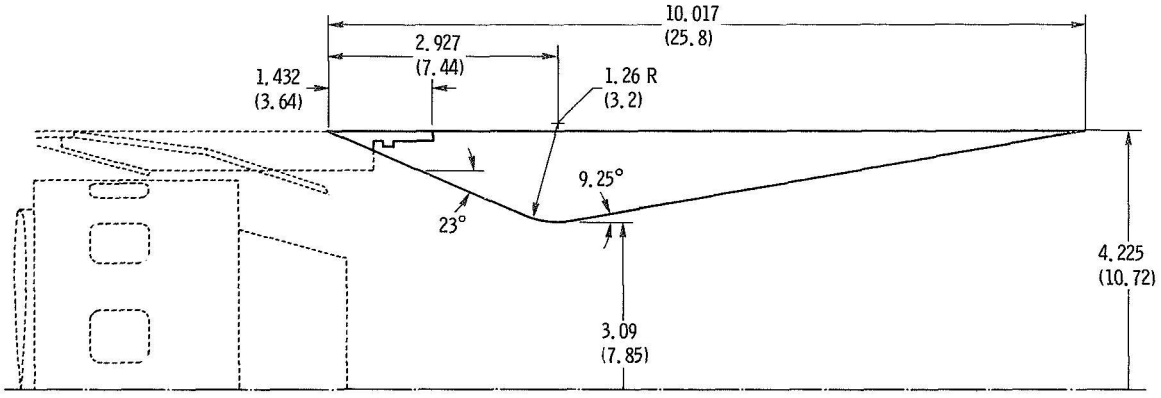

(b-1) Dimensions.

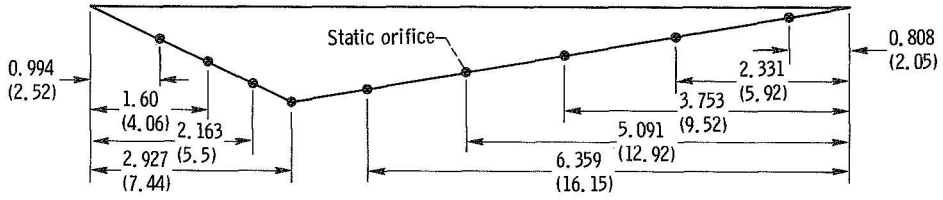

(b-2) Instrumentation.

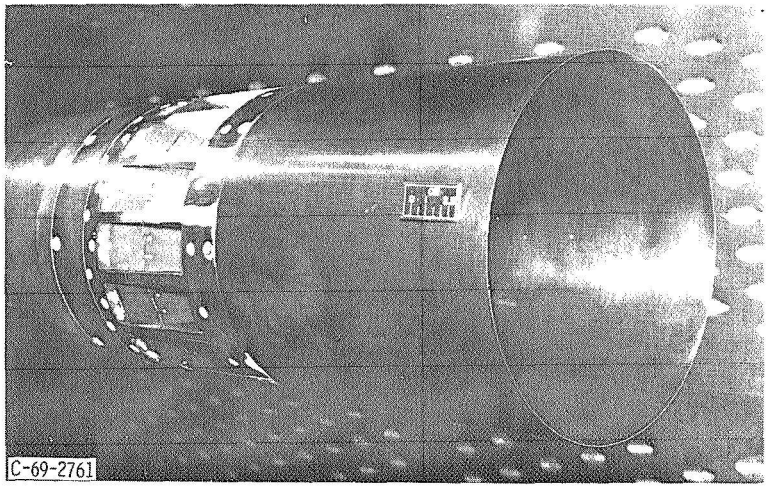

(b-3) Installed in wind tunnel

(b) Supersonic flap.

Figure 4. - Continued.

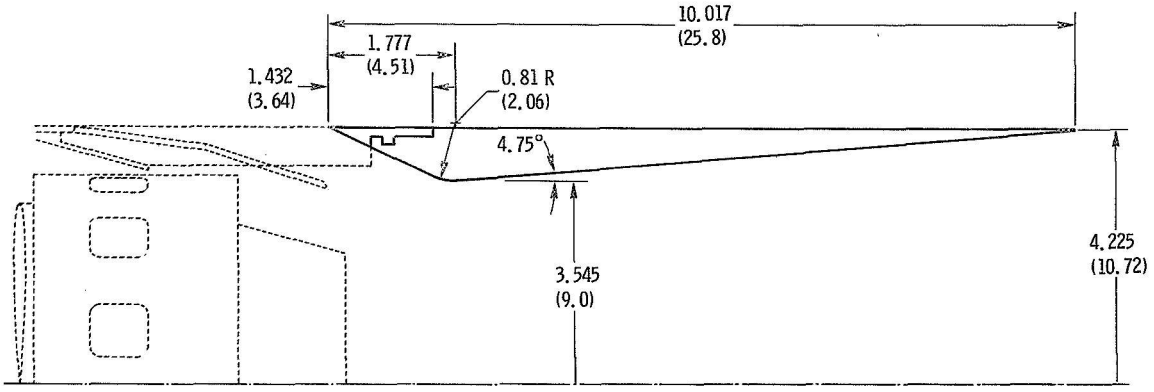

(c-1) Dimensions.

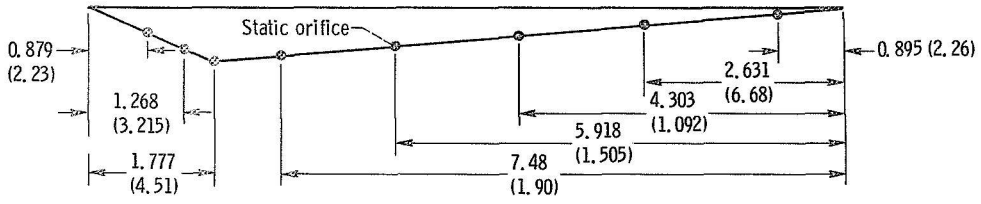

(c-2) Instrumentation

(c) Thin flap.

Figure 4. - Concluded.

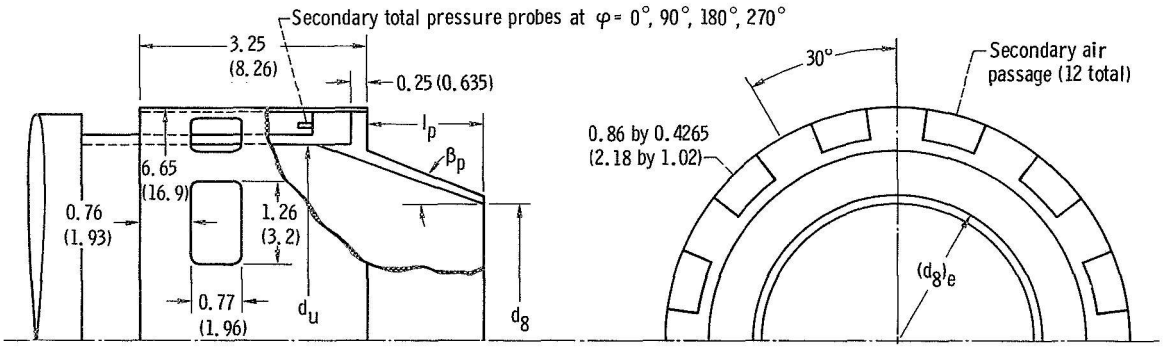

Primary nozzle length, l_p	Primary nozzle diameter, d_8	Primary nozzle boattail angle, β_p, deg	Primary nozzle throat flow coefficient $(C_d)_8$	Upstream diameter, d_u	Nozzle throat outside diameter, $(d_8)_e$
1.50 (3.81)	4.388 (11.146)	13.25	0.977	5.45 (13.85)	4.622 (11.74)
1.08 (2.743)	5.192 (13.188)	5.30	0.985	5.45 (13.85)	5.437 (13.81)

(a) Dimensions.

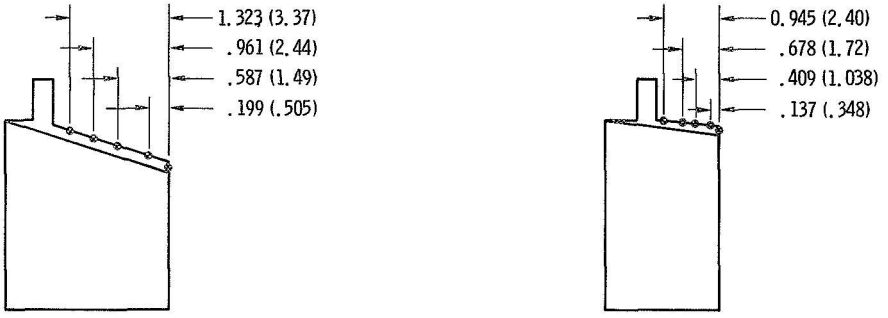

(b) Instrumentation.

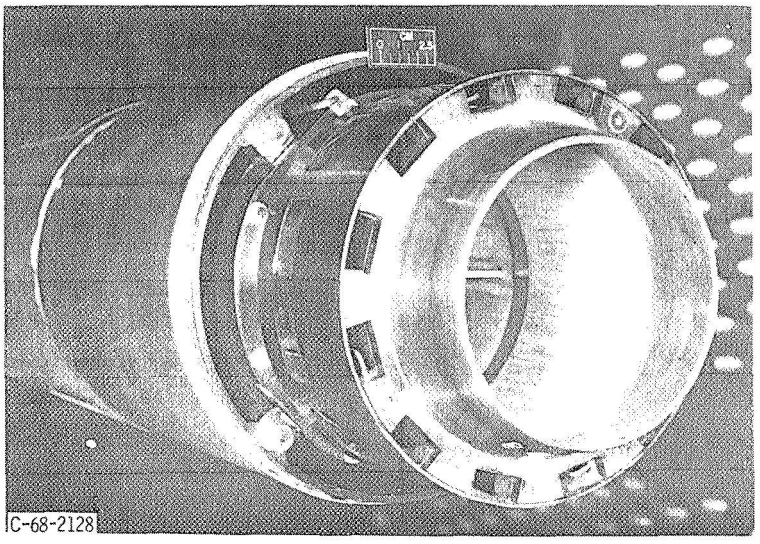

(c) Installed in wind tunnel.

Figure 5. - Details of simulated J85-GE-13 primary nozzle. Dimensions are in inches (cm).

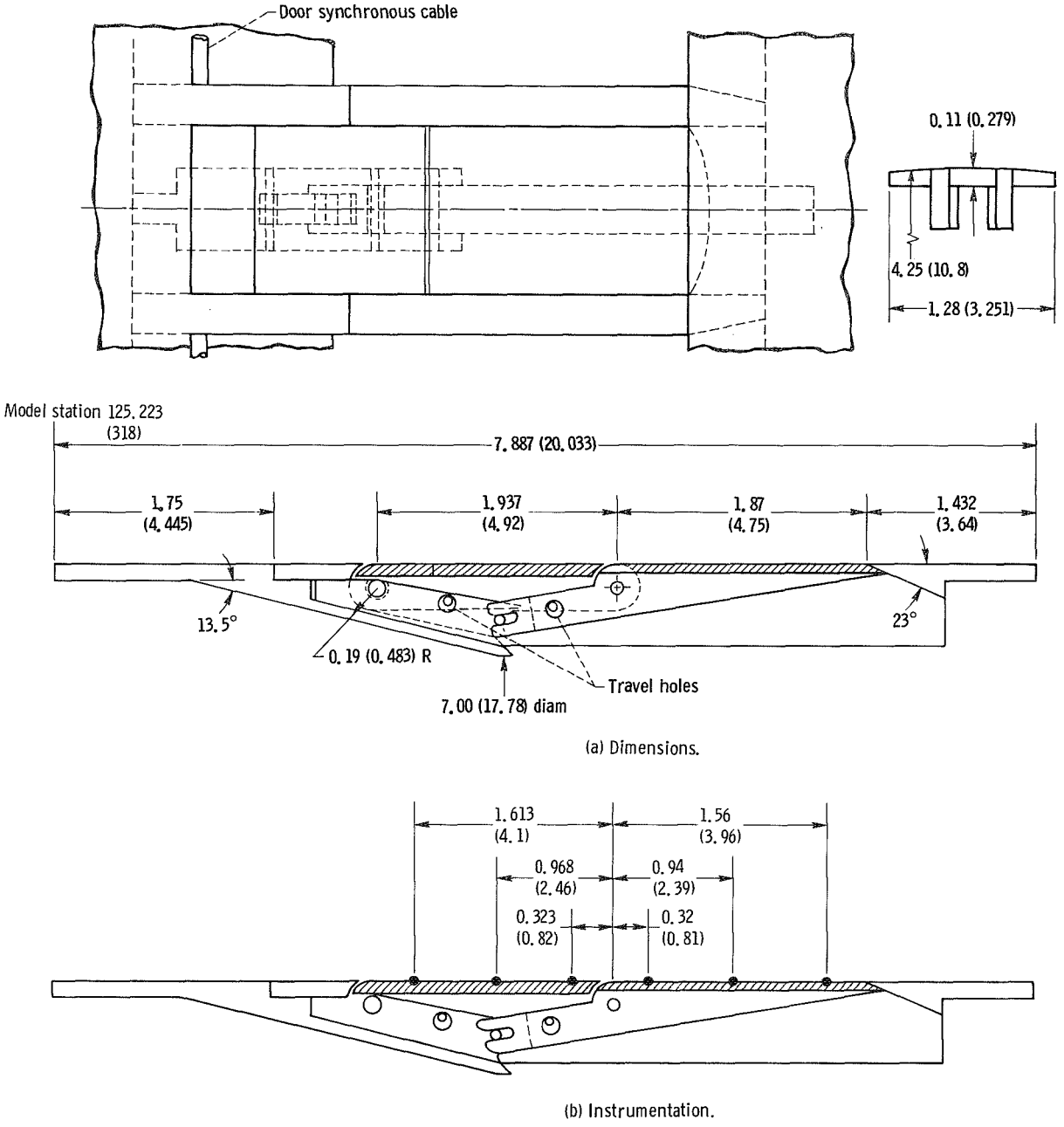

Figure 6. - Details of floating double-hinge door. Dimensions are in inches (cm).

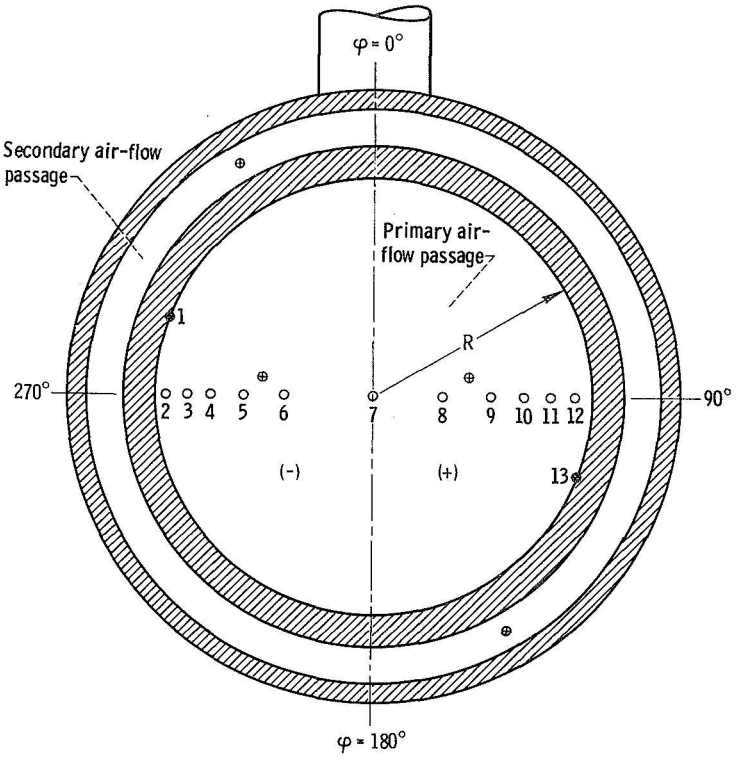

Primary flow orifice number	Normalized distance from centerline, r/R^a
1	-1.000
2	-.900
3	-.790
4	-.670
5	-.519
6	-.300
7	0
8	.418
9	.600
10	.750
11	.855
12	.950
13	1.000

[a] R = 3.006 in. (7.635 cm); r is radius from centerline to the local orifice.

⊗ Static-pressure
○ Total-pressure
⊕ Thermocouple

Figure 7. - Details of primary flow passage instrumentation at station 7. Dimensions are in inches (cm).

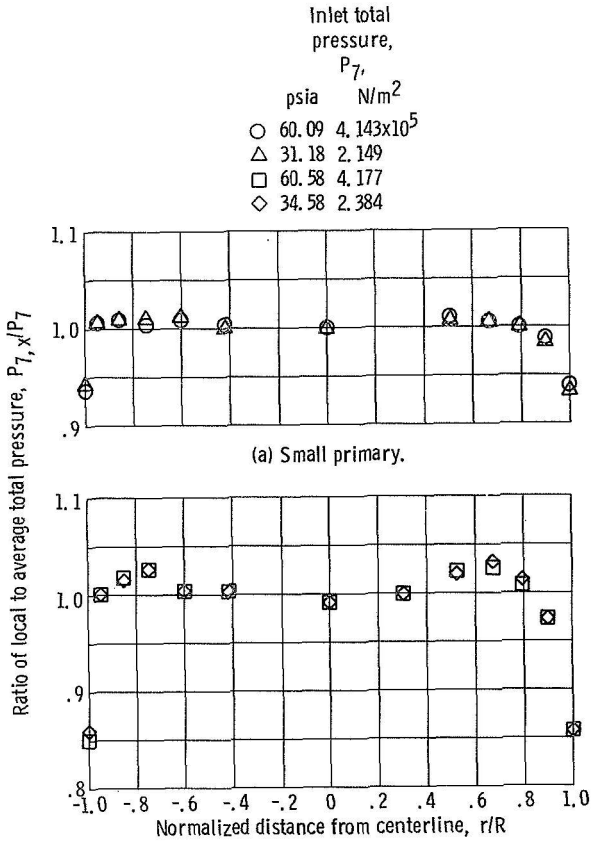

(a) Small primary.

(b) Large primary.

Figure 8. - Primary air total-pressure profile at station 7.

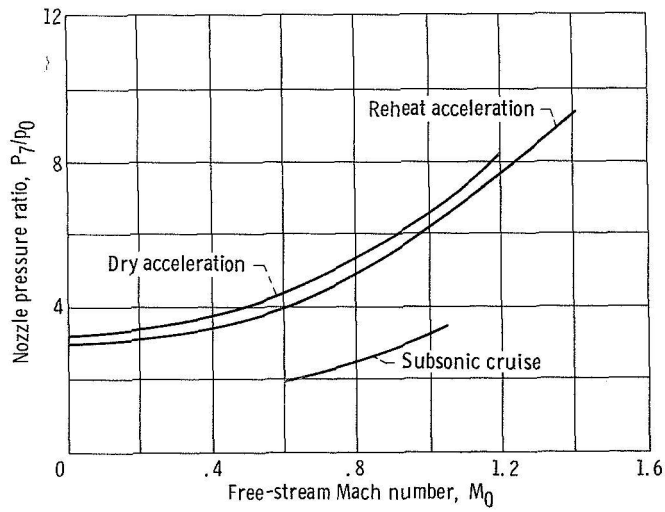

Figure 9. - Schedule of nozzle pressure ratio with free-stream Mach number.

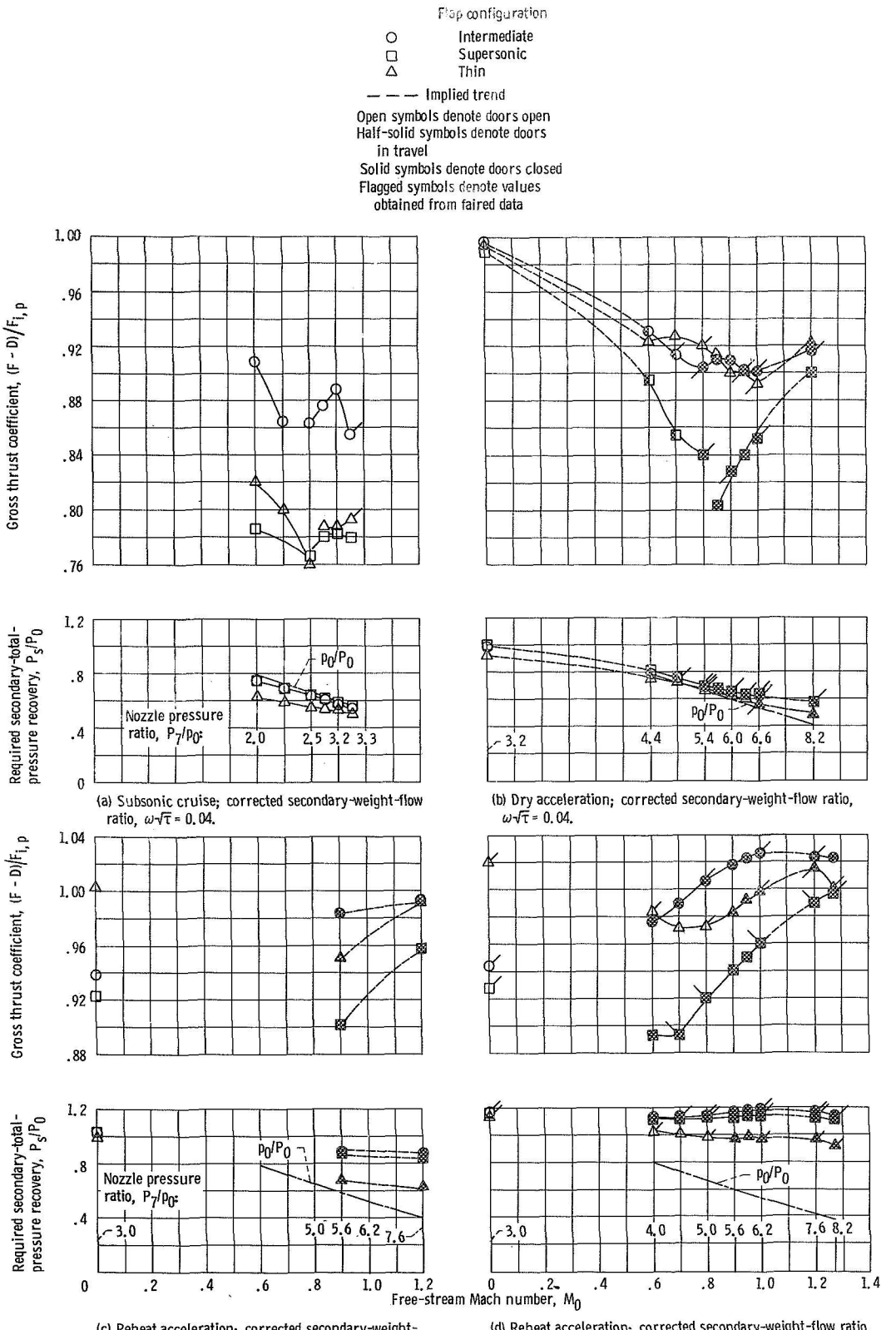

(a) Subsonic cruise; corrected secondary-weight-flow ratio, $\omega\sqrt{\tau} = 0.04$.

(b) Dry acceleration; corrected secondary-weight-flow ratio, $\omega\sqrt{\tau} = 0.04$.

(c) Reheat acceleration; corrected secondary-weight-flow ratio, $\omega\sqrt{\tau} = 0.04$.

(d) Reheat acceleration; corrected secondary-weight-flow ratio, $\omega\sqrt{\tau} = 0.08$.

Figure 10. - Effect of trailing-edge-flap geometry on nozzle performance and secondary total-pressure-recovery requirements.

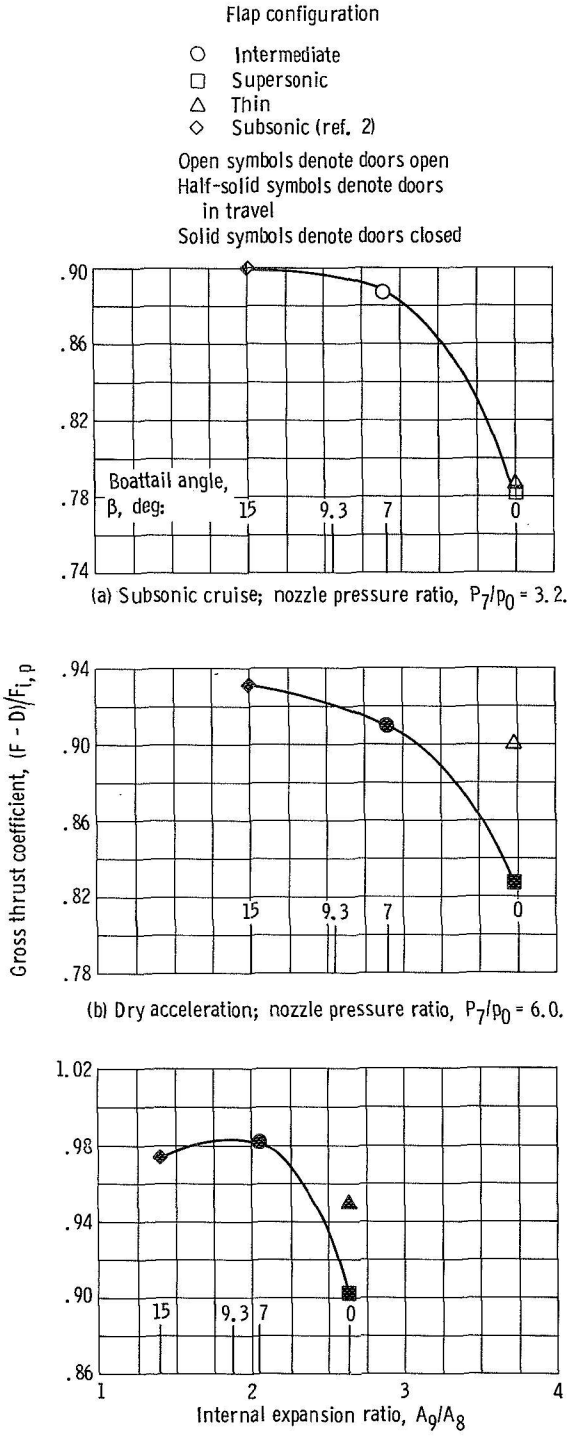

(a) Subsonic cruise; nozzle pressure ratio, $P_7/p_0 = 3.2$.

(b) Dry acceleration; nozzle pressure ratio, $P_7/p_0 = 6.0$.

(c) Reheat acceleration; nozzle pressure ratio, $P_7/p_0 = 5.6$.

Figure 11. - Effect of internal expansion ratio on nozzle gross thrust coefficient. Free-stream Mach number, $M_0 = 0.9$; corrected secondary-weight-flow ratio, $\omega\sqrt{\tau} = 0.04$.

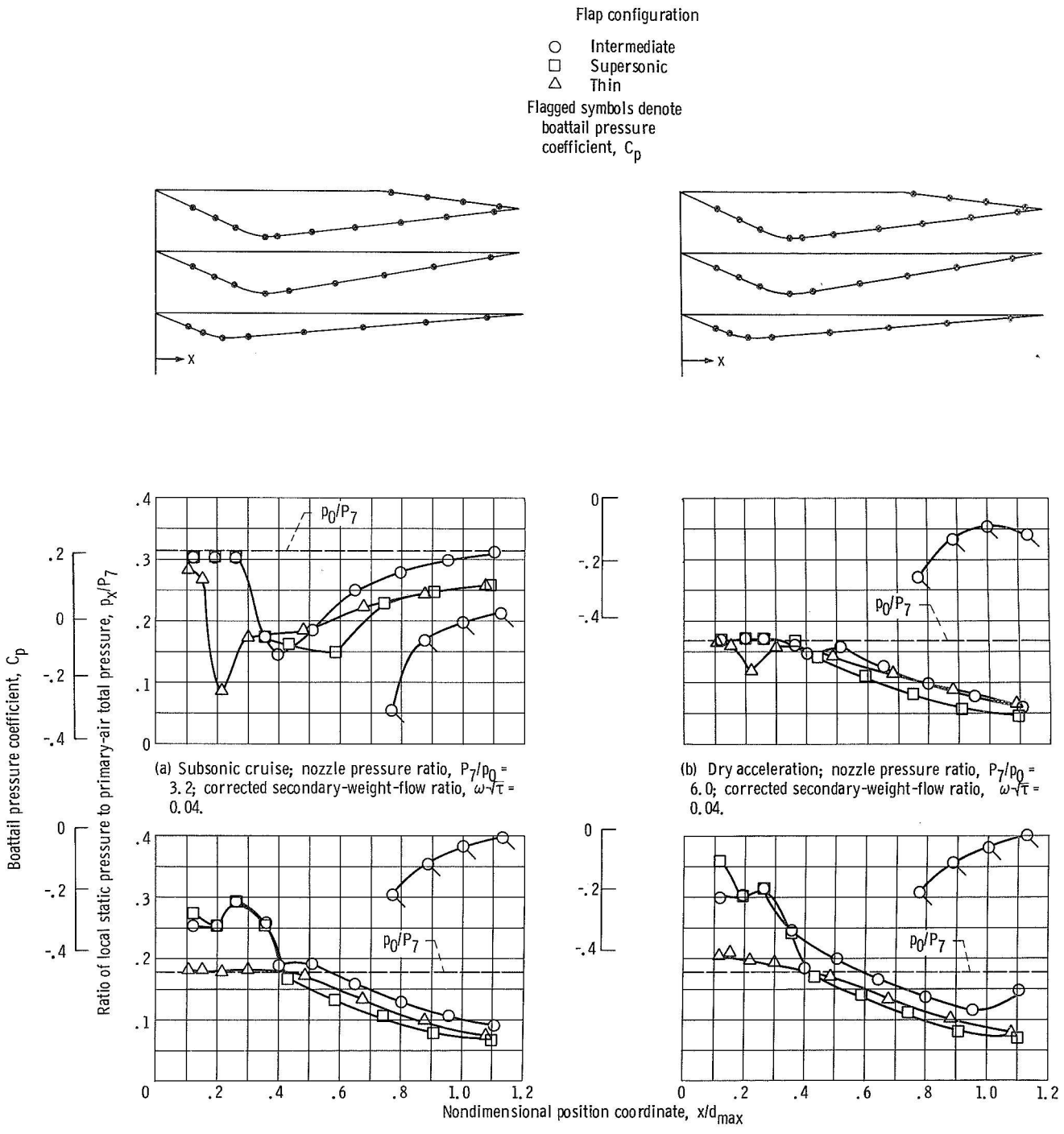

(a) Subsonic cruise; nozzle pressure ratio, P_7/p_0 = 3.2; corrected secondary-weight-flow ratio, $\omega\sqrt{\theta}$ = 0.04.

(b) Dry acceleration; nozzle pressure ratio, P_7/p_0 = 6.0; corrected secondary-weight-flow ratio, $\omega\sqrt{\theta}$ = 0.04.

(c) Reheat acceleration; nozzle pressure ratio, P_7/p_0 = 5.6; corrected secondary-weight-flow ratio, $\omega\sqrt{\theta}$ = 0.04.

(d) Reheat acceleration; nozzle pressure ratio, P_7/p_0 = 5.6; corrected secondary-weight-flow ratio, $\omega\sqrt{\theta}$ = 0.08.

Figure 12. - Flap pressure distributions; free-stream Mach number, M_0 = 0.9.

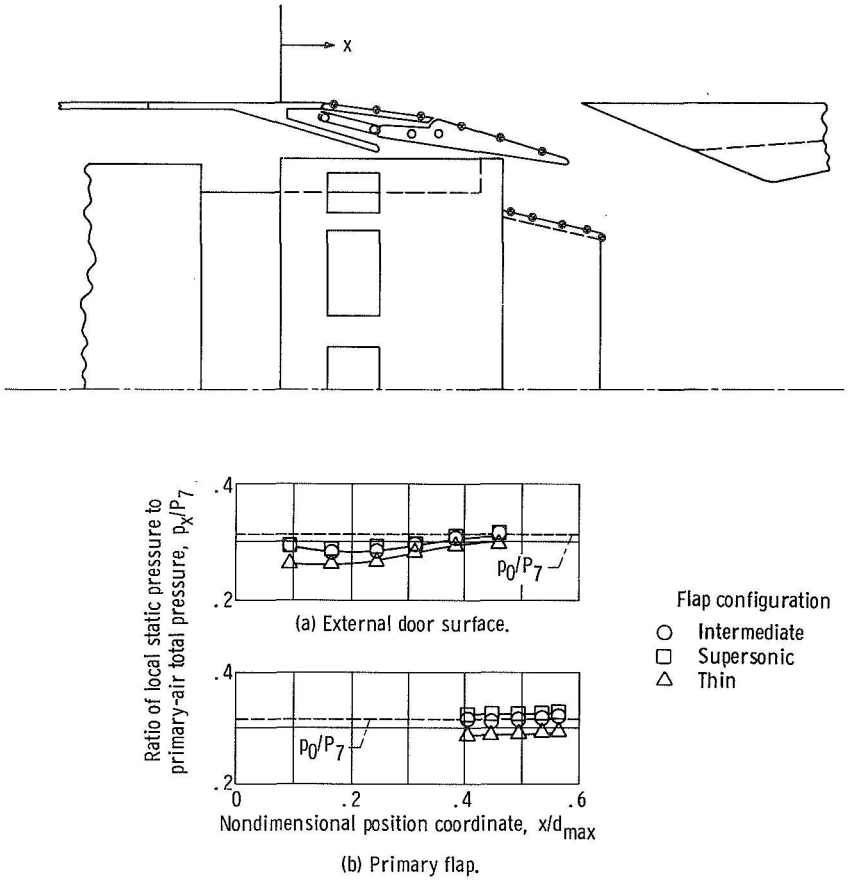

Figure 13. - Effect of trailing-edge-flap geometry on floating door and primary flap pressures at subsonic cruise; free-stream Mach number, $M_0 = 0.9$; nozzle pressure ratio, $P_7/p_0 = 3.2$; corrected secondary-weight-flow ratio, $\omega\sqrt{\tau} = 0.04$.

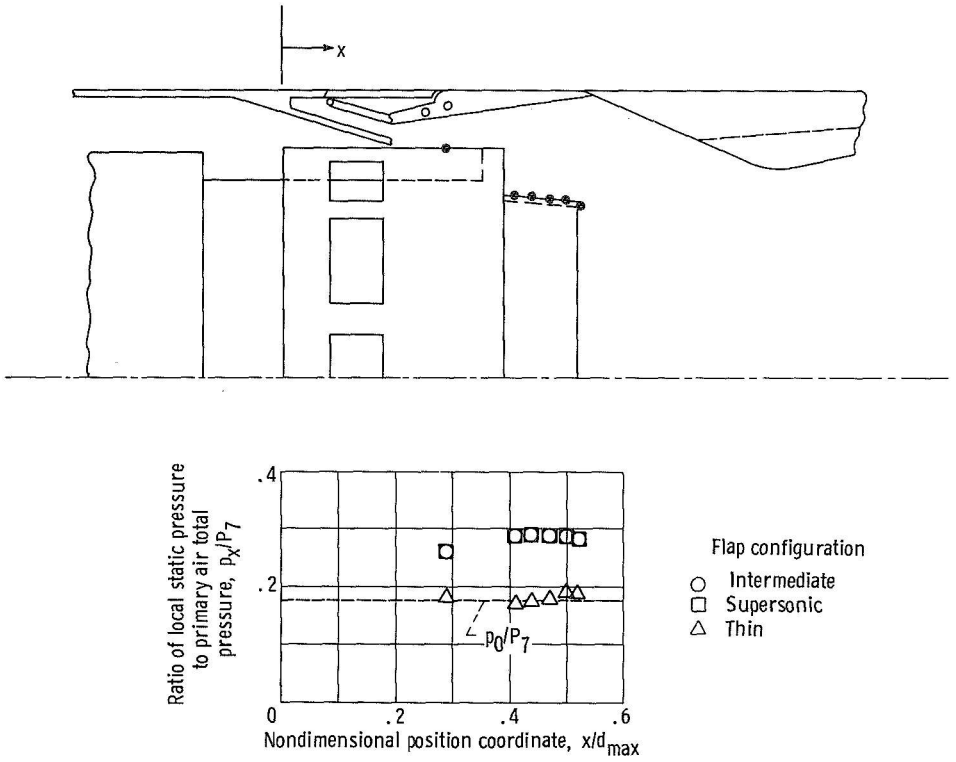

Figure 14. - Effect of trailing-edge-flap geometry on primary flap pressures at reheat acceleration; free-stream Mach number 0.9; nozzle pressure ratio, $P_7/p_0 = 5.6$; corrected secondary-weight-flow ratio, $\omega\sqrt{\tau} = 0.04$.

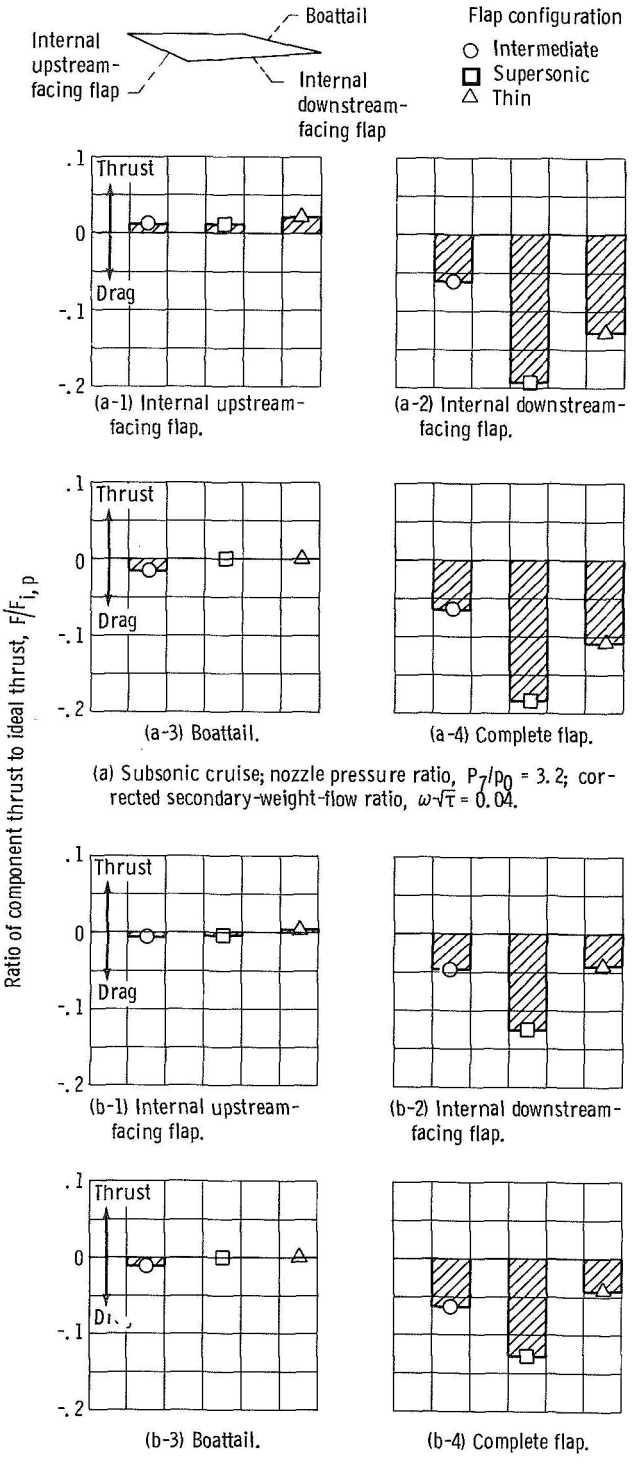

(a-1) Internal upstream-facing flap.

(a-2) Internal downstream-facing flap.

(a-3) Boattail.

(a-4) Complete flap.

(a) Subsonic cruise; nozzle pressure ratio, $P_7/p_0 = 3.2$; corrected secondary-weight-flow ratio, $\omega\sqrt{\tau} = 0.04$.

(b-1) Internal upstream-facing flap.

(b-2) Internal downstream-facing flap.

(b-3) Boattail.

(b-4) Complete flap.

(b) Dry acceleration; nozzle pressure ratio, $P_7/p_0 = 6.0$; corrected secondary-weight-flow ratio, $\omega\sqrt{\tau} = 0.04$.

Figure 15. - Trailing-edge-flap pressure forces at free-stream Mach number, $M_0 = 0.9$.

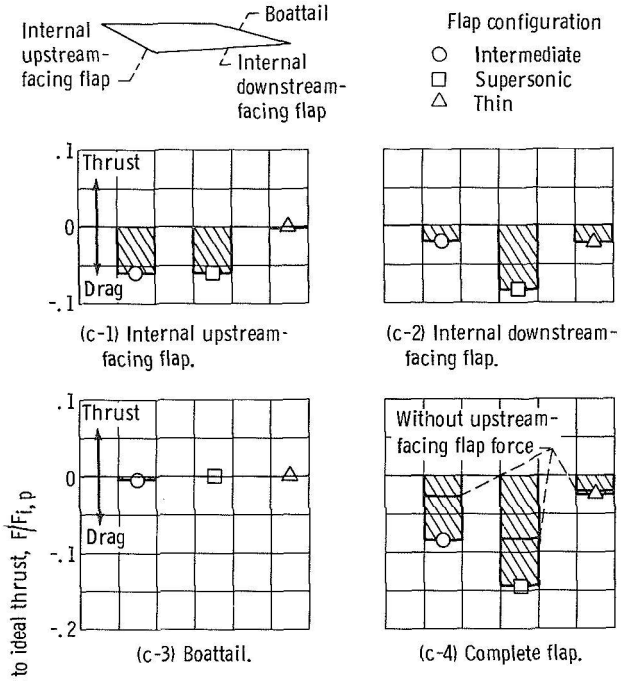

(c-1) Internal upstream-facing flap.

(c-2) Internal downstream-facing flap.

(c-3) Boattail.

(c-4) Complete flap.

(c) Reheat acceleration; nozzle pressure ratio, $P_7/p_0 = 5.6$; corrected secondary-weight-flow ratio, $\omega\sqrt{\tau} = 0.04$.

(d-1) Internal upstream-facing flap.

(d-2) Internal downstream-facing flap.

(d-3) Boattail.

(d-4) Complete flap.

(d) Reheat acceleration; nozzle pressure ratio, $P_7/p_0 = 5.6$; corrected secondary-weight-flow ratio, $\omega\sqrt{\tau} = 0.08$.

Figure 15. - Concluded.

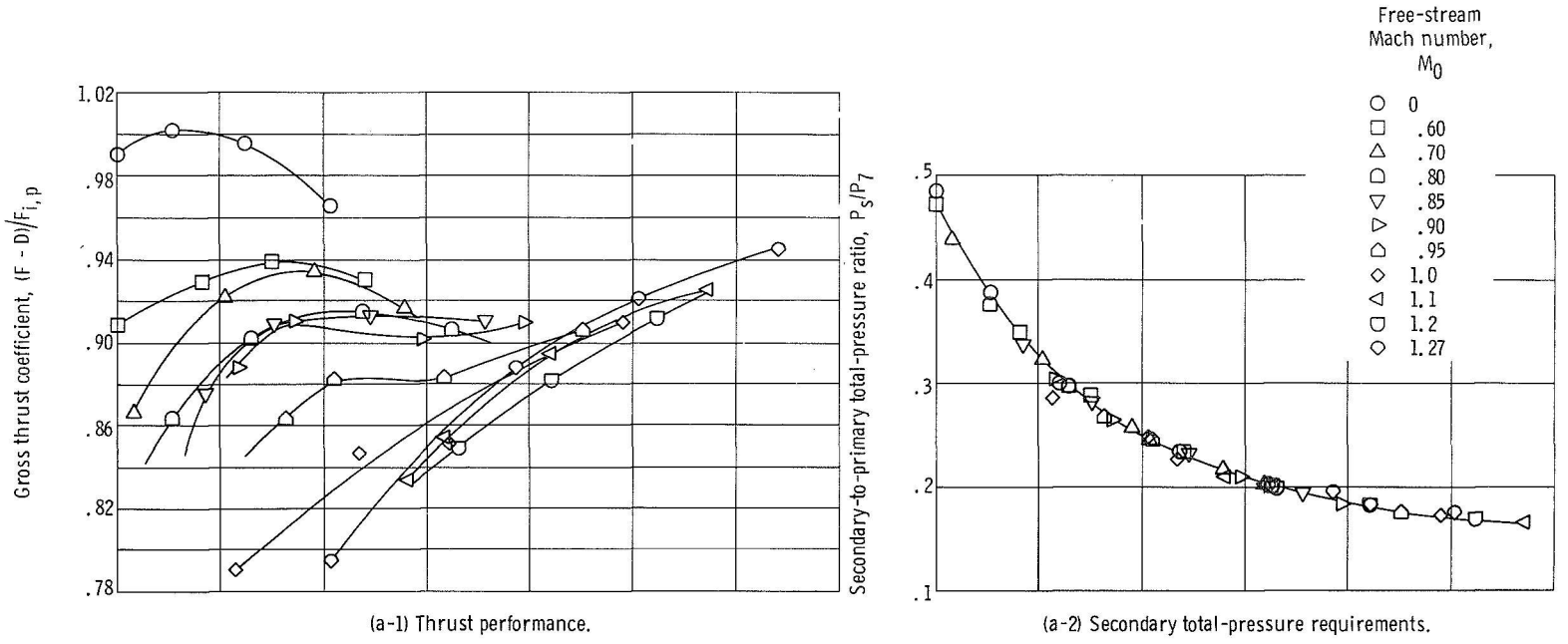

(a-1) Thrust performance.

(a-2) Secondary total-pressure requirements.

(a) Small primary; corrected secondary-weight-flow ratio, $\omega\sqrt{\tau} = 0.04$.

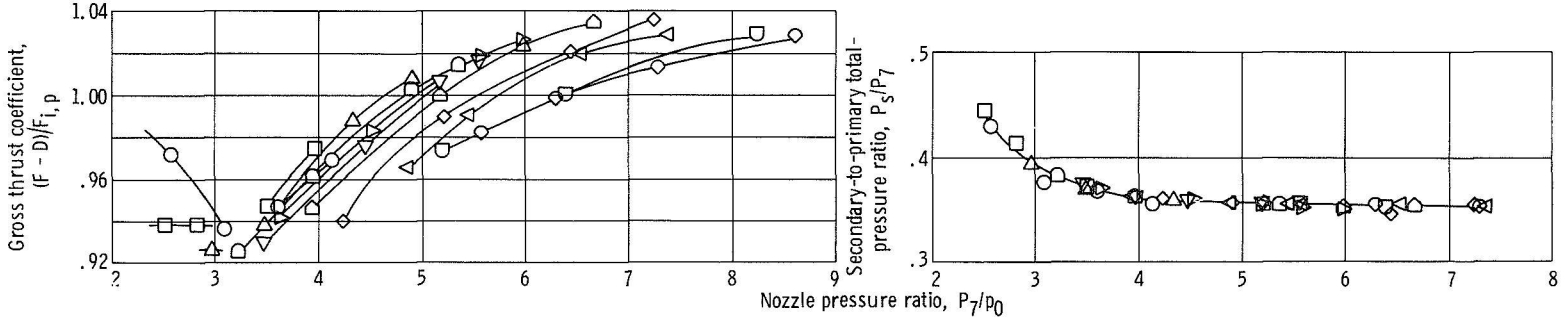

(b-1) Thrust performance.

(b-2) Secondary total-pressure requirements.

(b) Large primary; corrected secondary-weight-flow ratio, $\omega\sqrt{\tau} = 0.08$.

Figure 16. - Basic nozzle performance data as a function of nozzle pressure ratio with the intermediate trailing-edge flap.

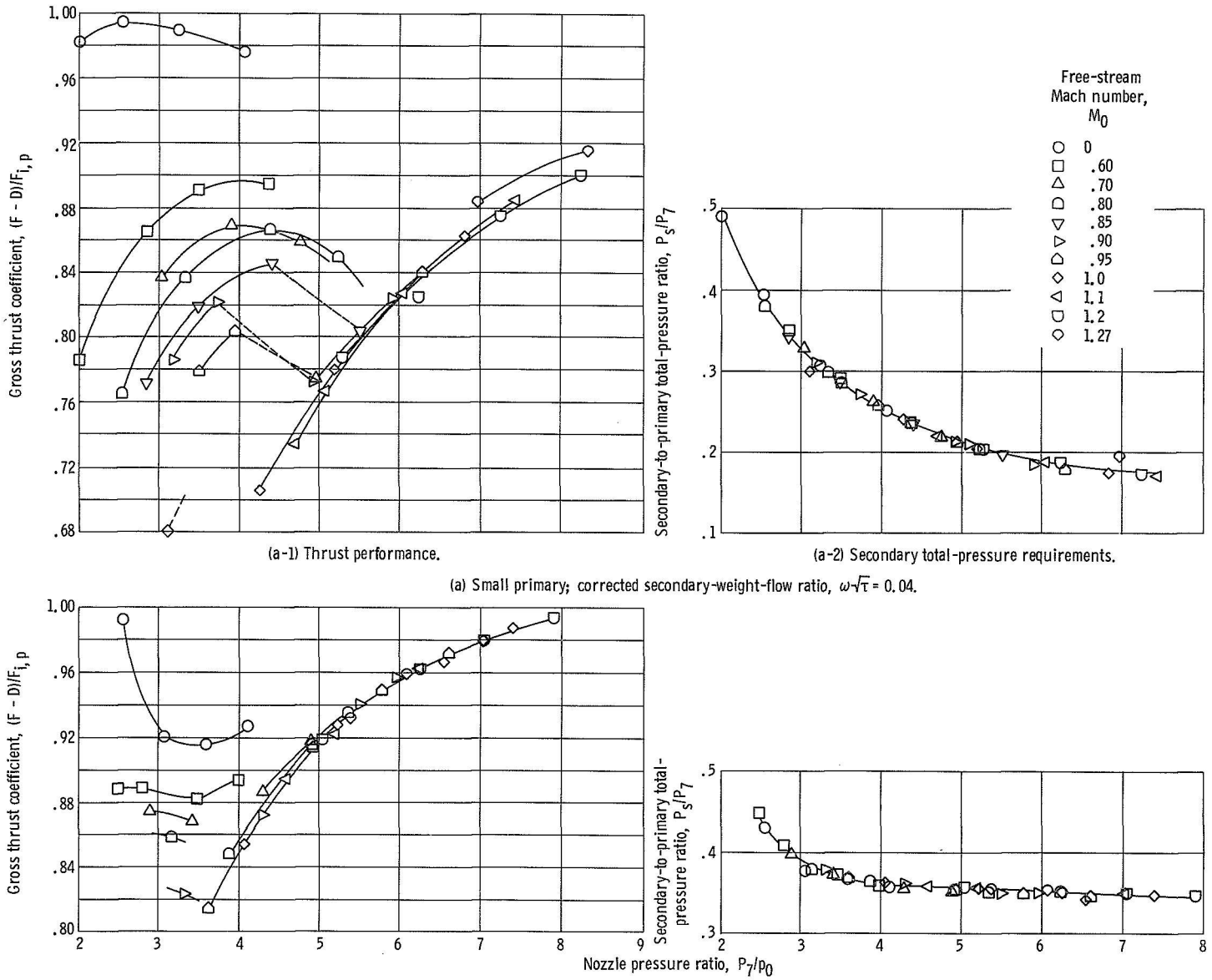

(a-1) Thrust performance.

(a-2) Secondary total-pressure requirements.

(a) Small primary; corrected secondary-weight-flow ratio, $\omega\sqrt{\tau} = 0.04$.

(b-1) Thrust performance.

(b-2) Secondary total-pressure requirements.

(b) Large primary; corrected secondary-weight-flow ratio, $\omega\sqrt{\tau} = 0.08$.

Figure 17. - Basic nozzle performance data as a function of nozzle pressure ratio with the supersonic trailing-edge flap.

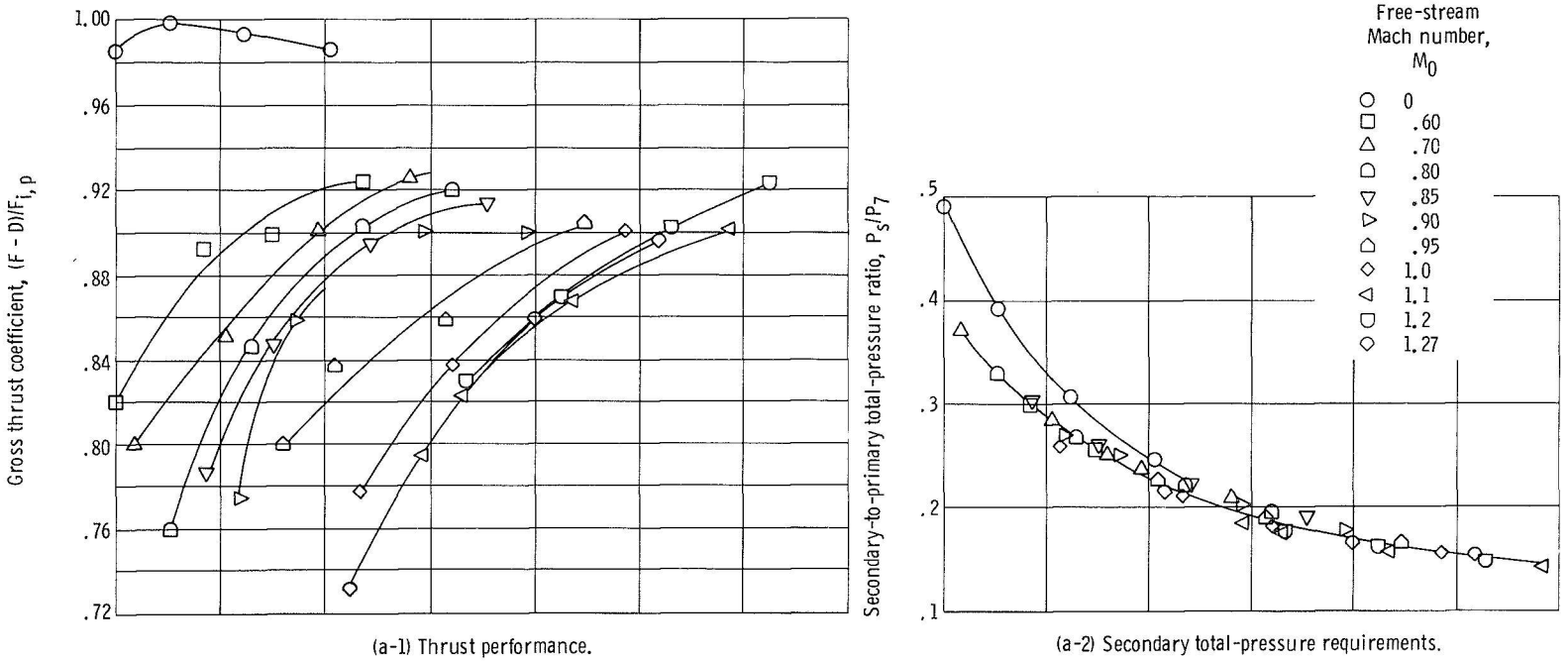

(a-1) Thrust performance.

(a-2) Secondary total-pressure requirements.

(a) Small primary; corrected secondary-weight-flow ratio, $\omega\sqrt{\tau} = 0.04$.

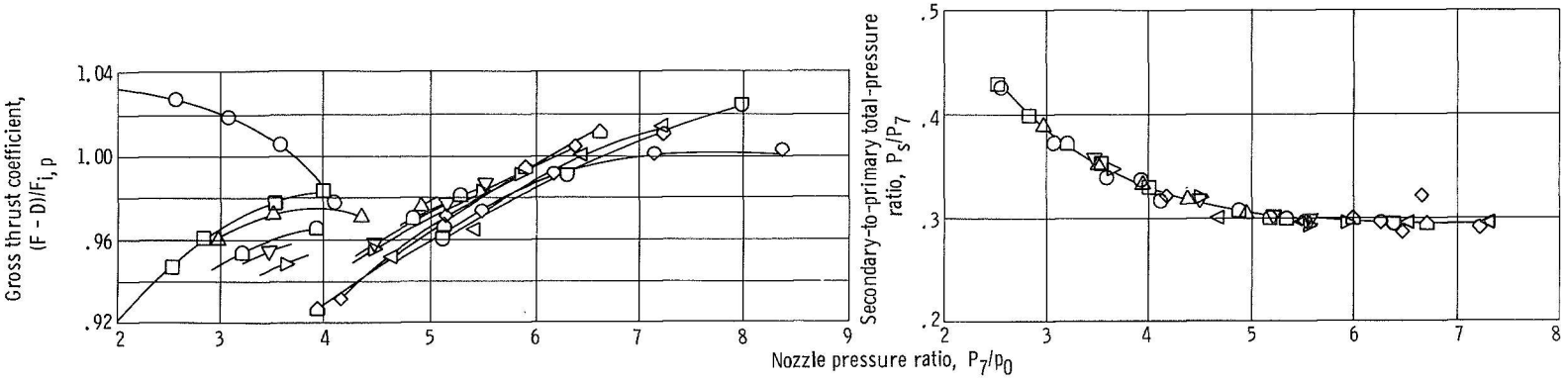

(b-1) Thrust performance.

(b-2) Secondary total-pressure requirements.

(b) Large primary; corrected secondary-weight-flow ratio, $\omega\sqrt{\tau} = 0.08$.

Figure 18. - Basic nozzle performance data as a function of nozzle pressure ratio with the thin trailing-edge flap.

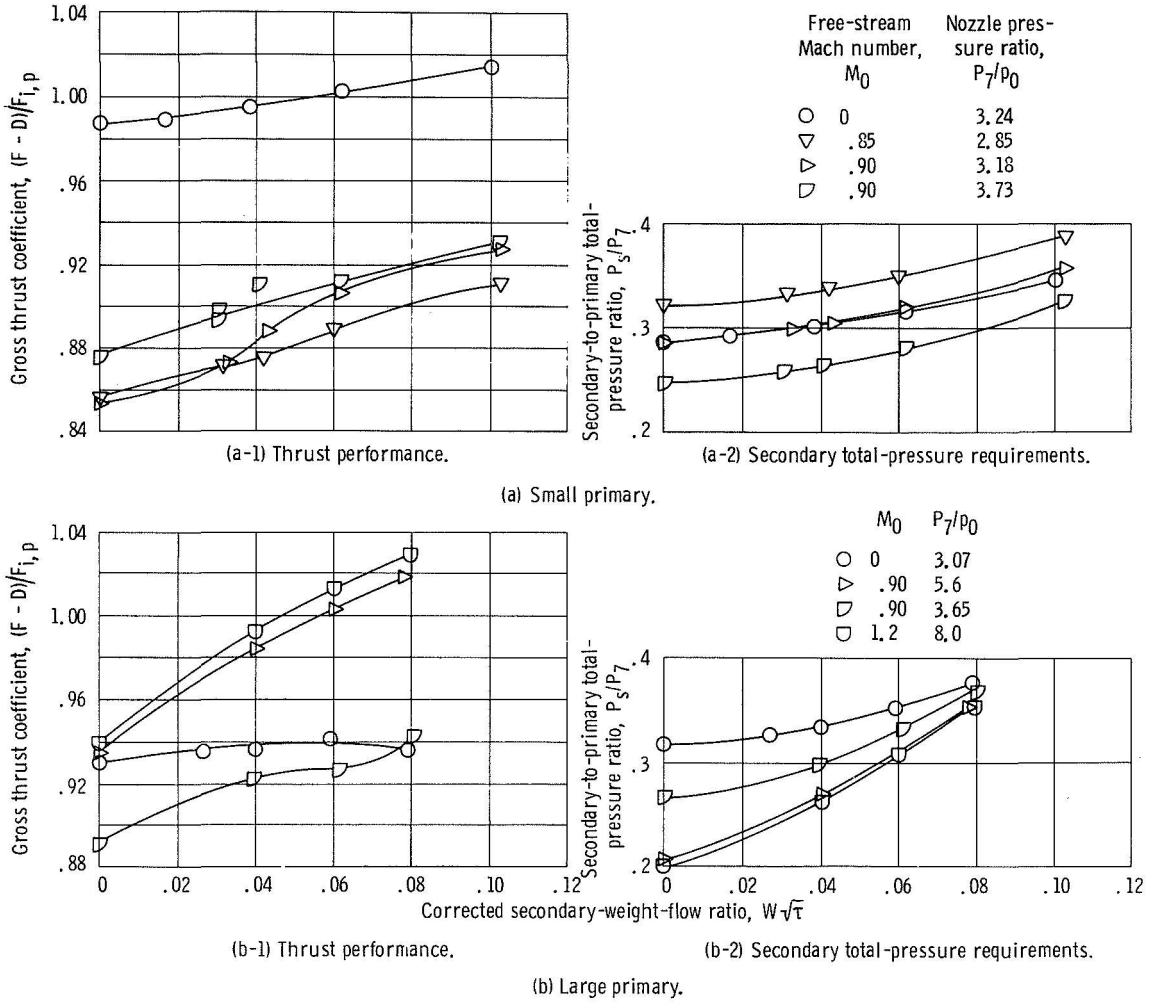

Figure 19. - Basic nozzle performance data as a function of corrected secondary-weight-flow ratio with the intermediate trailing-edge flap.

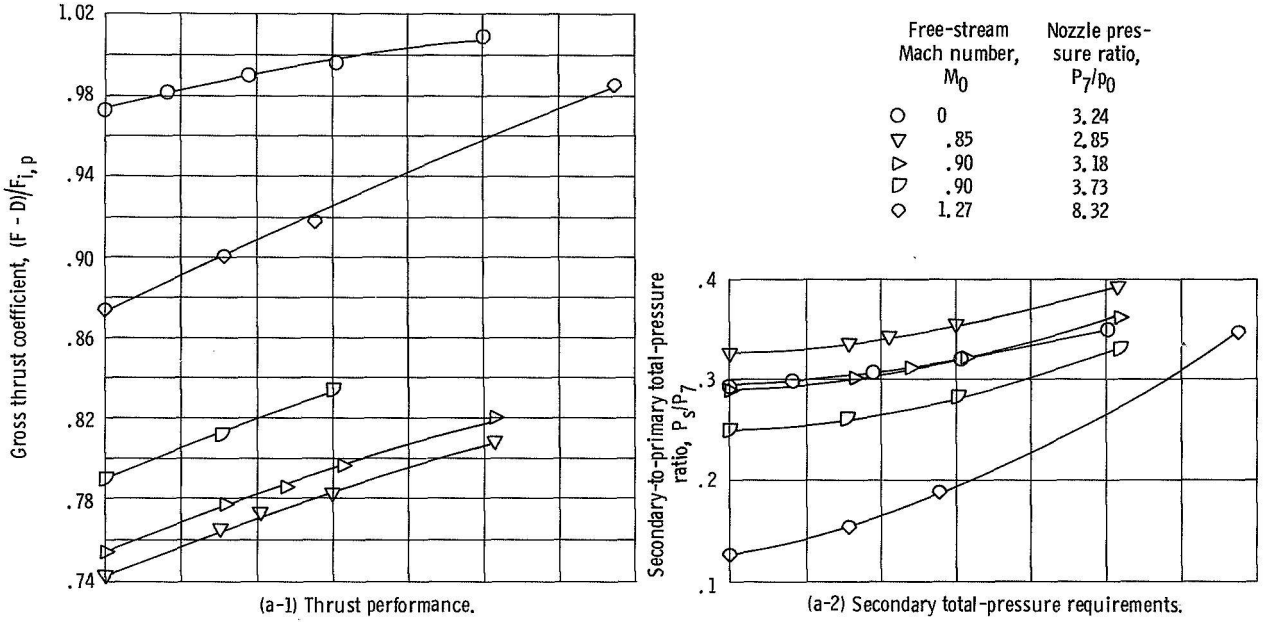

(a-1) Thrust performance.

(a-2) Secondary total-pressure requirements.

(a) Small primary.

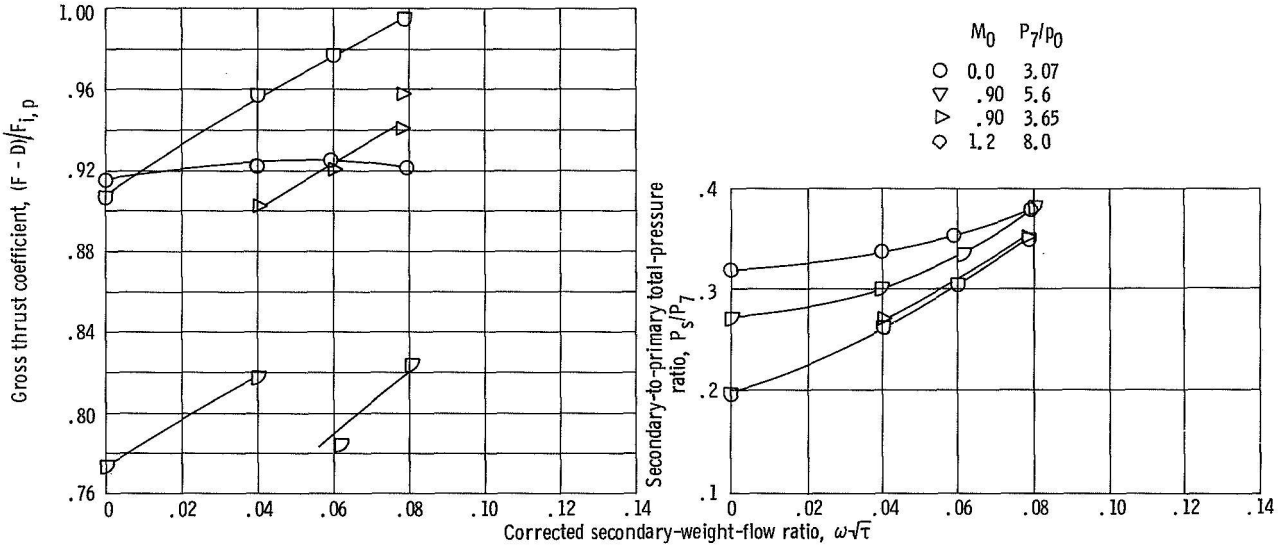

(b-1) Thrust performance.

(b-2) Secondary total-pressure requirements.

(b) Large primary.

Figure 20. - Basic nozzle performance data as a function of corrected secondary-weight-flow ratio with the supersonic trailing-edge flap.

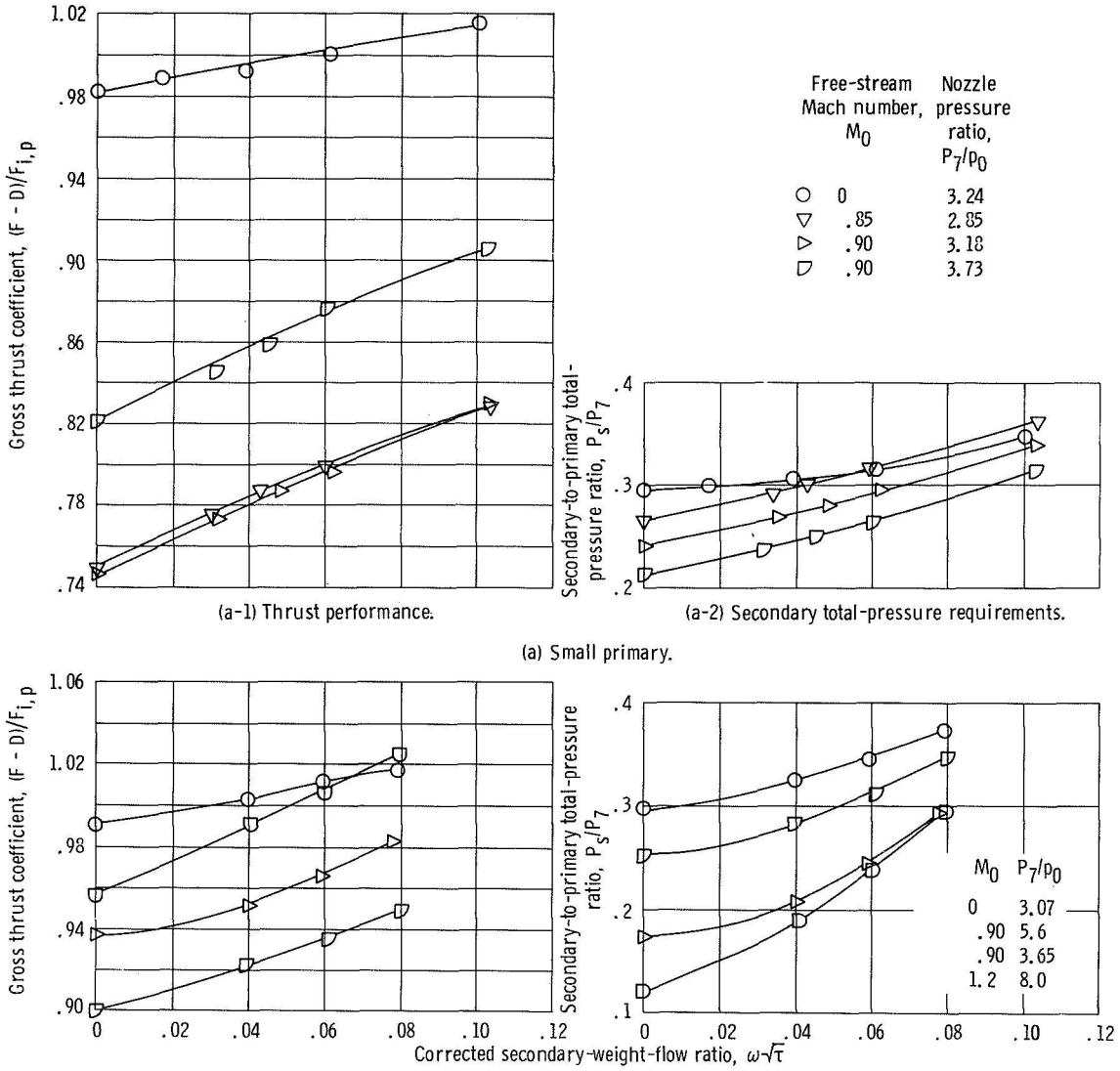

Figure 21. - Basic nozzle performance data as a function of corrected secondary-weight-flow ratio with the thin trailing-edge flap.

NATIONAL AERONAUTICS AND SPACE ADMINISTRATION
WASHINGTON, D.C. 20546

OFFICIAL BUSINESS

FIRST CLASS MAIL

POSTAGE AND FEES PAID
NATIONAL AERONAUTICS AN
SPACE ADMINISTRATION

POSTMASTER: If Undeliverable (Section 158
Postal Manual) Do Not Return

"The aeronautical and space activities of the United States shall be conducted so as to contribute . . . to the expansion of human knowledge of phenomena in the atmosphere and space. The Administration shall provide for the widest practicable and appropriate dissemination of information concerning its activities and the results thereof."

— NATIONAL AERONAUTICS AND SPACE ACT OF 1958

NASA SCIENTIFIC AND TECHNICAL PUBLICATIONS

TECHNICAL REPORTS: Scientific and technical information considered important, complete, and a lasting contribution to existing knowledge.

TECHNICAL NOTES: Information less broad in scope but nevertheless of importance as a contribution to existing knowledge.

TECHNICAL MEMORANDUMS: Information receiving limited distribution because of preliminary data, security classification, or other reasons.

CONTRACTOR REPORTS: Scientific and technical information generated under a NASA contract or grant and considered an important contribution to existing knowledge.

TECHNICAL TRANSLATIONS: Information published in a foreign language considered to merit NASA distribution in English.

SPECIAL PUBLICATIONS: Information derived from or of value to NASA activities. Publications include conference proceedings, monographs, data compilations, handbooks, sourcebooks, and special bibliographies.

TECHNOLOGY UTILIZATION PUBLICATIONS: Information on technology used by NASA that may be of particular interest in commercial and other non-aerospace applications. Publications include Tech Briefs, Technology Utilization Reports and Technology Surveys.

Details on the availability of these publications may be obtained from:

SCIENTIFIC AND TECHNICAL INFORMATION OFFICE

NATIONAL AERONAUTICS AND SPACE ADMINISTRATION

Washington, D.C. 20546